

Chapter 1

Introduction

The term nanotechnology refers to the use of structures that have novel properties with at least one dimension less than 100 nm^[1]. If all three dimensions of a structure lie in 1-100 nm range, then it is considered to be a nanoparticle. Typically, nanoparticles are composed of atoms or molecules bonded together (10^6 atoms or fewer), having sizes intermediate between that of individual atoms and bulk material. Because the nanoparticles are bigger than the individual atoms or molecules but are smaller than the bulk solid, materials in the nanometre size range show properties which are intermediate between atomic or molecular structures and macroscopic solids. The main factors that are responsible for these variations are surface to volume ratio, quantum size effects and changes in morphology of the crystal structure^[2].

Metal nanoparticles possess unique optical, electrical, chemical and magnetic properties that have attracted the attention of researchers for applications in catalysis, medicine, biology, electronics, etc^[2,3]. Bioconjugated gold and silver nanoparticles are candidates for the detection of biomolecules and chemical species^[4]. Gold nanoparticles supported on Co_3O_4 , Fe_2O_3 or TiO_2 act as highly active catalysts for CO and H_2 oxidation, NO reduction, water gas shift reaction, CO_2 hydrogenation and combustion of methanol^[5].

Several methods have been reported for the synthesis of metal nanoparticles in the literature. These methods can be classified into gas phase synthesis and liquid phase synthesis routes. The gas phase synthesis process involves evaporation of the bulk material using high energy sources such as resistive heaters or lasers to obtain a supersaturated gas phase, which under controlled conditions forms nuclei that grow to become nanoparticles. In liquid phase or wet synthesis methods, nanoparticle synthesis involves reduction of the metal precursor salts into metal atoms to form supersaturated solutions, which undergo nucleation and growth to form nanoparticles. Compared to gas phase methods, wet synthesis methods are more energy efficient and do not require sophisticated vacuum equipment^[6].

Different methods are available for the preparation of monodisperse nanoparticles in batch reactors. All the methods follow a fixed protocol for synthesising nanoparticles of definite mean size and polydispersity. A slight change in protocol results in particles of unexpected quality. Reproducibility and scale up of the synthesis to produce large quantities of the particles are challenging issues. Nanoparticles synthesis in microfluidic devices gives particles with reproducible results, better mean size and polydispersity^[7,8]. These devices allow controlled mixing through diffusion mediated transport and gives controlled nucleation and growth of the nanoparticles. Local variations in reaction conditions such as concentration and temperature can also be eliminated^[8]. Control of nanoparticle synthesis in continuous flow reactors can be expected only through the understanding of the kinetics and modeling of nanoparticle formation in batch reactors.

The main objective of this project is to understand the kinetics of gold salt reduction, and gold nanoparticle formation synthesised by redox reactions and to implement tools for deconvolution of UV-Vis spectroscopic data for better understanding of gold salt reduction and nanoparticle formation. Another objective is to identify appropriate models that capture kinetics of nanoparticles formation and evaluate them. A stopped flow module (SFM-400) from Biologic SAS, France equipped with a diode array spectrophotometer was used to gather UV-Vis spectroscopic data at rapid rate during nanoparticle formation. The diode array spectrophotometer gives 3D-spectra (wavelength-absorbance-time) and analysis of these spectra to obtain information corresponding to the various evolving species was carried out using multivariate curve resolution–alternating least squares method (MCR – ALS). This enabled us to infer the kinetics of the both gold salt reduction and nanoparticle formation.

This project report is organised in the following way. After the introduction, background on formation of nanoparticles and literature review on kinetics of nanoparticles formation is presented in chapter 2. Chapter 3 is a brief discussion about the MCR-ALS method, followed by the application of this method to analyse the data obtained during gold nanoparticle formation by citrate reduction method. Experimental results obtained for kinetics of gold nanoparticles formation is presented

in chapter 4. Chapter 5 presents modeling of formation of gold nanoparticles by tannic acid method. A brief summary and recommendations for future work is presented in chapter 6.

1.1 References

- [1]. Booker R, Boysen E (2005) Nanotechnology for dummies. Wiley Publishing.
- [2]. Ghosh S K, Pal T (2007) Interparticle coupling effect on the surface plasmon resonance of gold nanoparticles: From theory to applications. *Chemical Reviews* 107:4797-4862.
- [3]. Salata O V (2004) Applications of nanoparticles in biology and medicine. *Journal of Nanobiotechnology* 2:1-6.
- [4]. Biju V, Ltoh T, Anas A (2008) Semiconductor quantum dots and metal nanoparticles: Syntheses, optical properties and biological applications. *Analytical and Bioanalytical Chemistry*.
- [5]. Daniel M, Astruc D (2004) Gold nanoparticles: Assembly, supramolecular chemistry, quantum-size-related properties, and applications toward biology, catalysis, and nanotechnology. *Chemical Reviews* 104:293-346.
- [6]. Kumar S, Gandhi K S, Kumar R (2007) Modeling of formation of gold nanoparticles by citrate method. *Industrial Engineering Chemistry and Research* 46:3128-3136.
- [7]. J. Wagner, and J. M. Kohler (2005) Continuous synthesis of gold nanoparticles in a microreactor . *Nano Letters* 5: 685-691.
- [8]. David S, Robert C.R. Wootton, Richard F. Winkle, Ben F. Cottam, Ramon Vilar, Andrew J. deMello, C. Paul Wilde (2007) Synthesis of thiol functionalized gold nanoparticles using a continuous flow microfluidic reactor. *Materials Letters* 61: 1146–1150.

- [9]. Chakraborty J (2008) Modeling and simulation frameworks for synthesis of nanoparticles. PhD Thesis, Indian Institute of Science.

Chapter 2

Background and Literature Review

Crystallization involves both nucleation and growth steps. Reaction crystallization differs from the normal classical crystallization process in that the supersaturation required for crystallization is achieved not simply by changing the physical properties of the system, rather it is generated by a chemical reaction^[1].

2.1 Preparation of monodisperse hydrosols

La Mer et al.^[2] studied the concentration changes of molecular sulphur during reaction crystallization from dilute aqueous solutions of hydrochloric acid and sodium thiosulfate and proposed a model for reaction crystallization. Figure 2.1 qualitatively shows concentration of molecularly dissolved sulfur during this process. Initially, as the reaction progresses, the concentration of molecular sulfur increases in the system and reaches a saturation limit (C_s). Further progress of the reaction increases it to a critical supersaturation (C_{crit}) value, where appreciable extent of nucleation starts. At this stage the rate of nucleation is low compared to rate of reaction, so, concentration of sulphur builds up for some more time. As the concentration of sulfur increases, the rate of nucleation accelerates and reaches a point where the consumption of molecular sulphur by nucleation is equal to its generation by reaction. Afterwards the rate of reaction decreases compared to nucleation because of the decrease in the concentration of the precursors. So, the concentration of sulphur falls and reaches the critical supersaturation (C_{crit}) value beyond which growth phase starts. Growth phase continues until the supersaturation is exhausted. To form monodispersed hydrosols the duration of nucleation stage should be very small (neglecting coagulation at later stages).

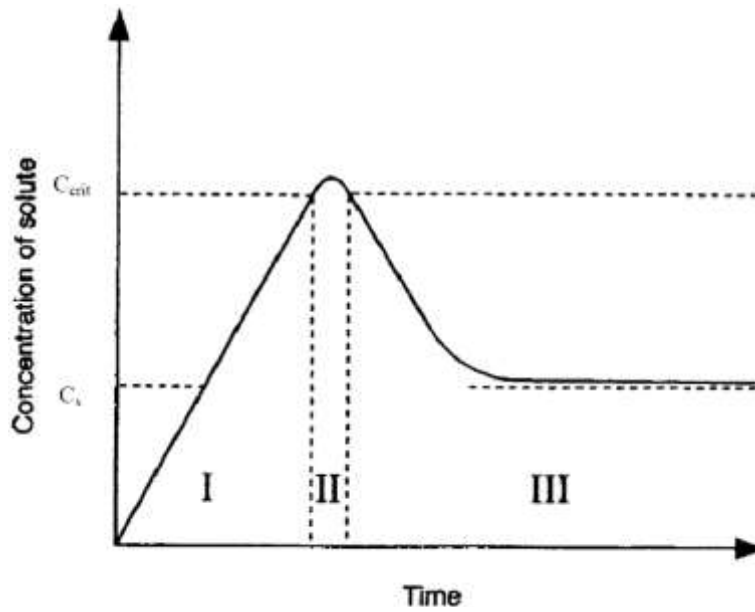


Fig. 2.1 Schematic representation of concentration of molecular sulfur in a reactive crystallization process. Stage I: Concentration of the sulfur increases due to chemical reaction. Stage II: Rapid nucleation takes place after it crosses a critical concentration threshold. Stage III: Growth of the nuclei will occur till supersaturation is exhausted^[2].

2.2 Nucleation models

The requirement for monodisperse nanoparticles to be formed is that nucleation should occur over a short duration. This is feasible if nucleation rate is a very sensitive function of supersaturation. Generally, classical nucleation theory (CNT) is invoked “to satisfy the equilibrium condition at all steps” in formation of critical cluster from supersaturated solution. The rate of the nucleation (N) i.e. the number of nuclei formed per unit volume per unit time is given by the following expression^[3]

$$N = A \exp \left[-\frac{16\pi\gamma^3 v^2}{3k^3 T^3 (\ln S)^2} \right] \quad (2.1)$$

where A is prefactor, γ is interfacial tension between solid surface and supersaturated solution, v is molecular volume of the solute, k is Boltzmann constant, T is absolute temperature of the solution and S is supersaturation ratio which is defined as the ratio of the concentration of the solute to the concentration of the solute at saturation. The

main drawback with CNT is that a single set of parameters satisfy experimental data over a very narrow range of conditions^[4].

Christiansen and Nielsen^[5] proposed a kinetic based mechanism for the formation of the nuclei from supersaturated solution and it satisfies the following equation

$$tA^{n-1} = \text{constant} \quad (2.2)$$

where t is nucleation time, A is concentration of the solute monomer and n is number of molecules in the critical cluster. The main difference is that the discrete atomic nature of matter is accounted for in kinetic model while CNT predicts a continuous change in number of monomers. The value of n in kinetics model has to obtain experimentally and it again varies with supersaturation.

The organizer mechanism of nucleation was first proposed by Turkevich et al.^[6] to explain the process of formation of colloidal gold from its precursors chloroauric acid and citrate. In this case, a nucleating agent which is formed by the oxidation of the reducing agent gradually forms a complex with gold ions and grows into a large macromolecule that then, undergoes a molecular rearrangement to form a nucleus. Such an organizer based mechanism has been used to quantitatively model gold nanoparticle formation and its steep variation with the initial molar ratio of citrate to chloroauric acid^[7]. Chakraborty has also proposed a general framework based on this concept that was used to quantitatively predict nanoparticle size variation during the reduction of gold chloride by mixture of tannic acid and citrate at 60°C^[4].

2.3 Growth mechanisms

Once a stable nucleus forms, it grows by the transfer of the solute monomers from the bulk solution to the surface of the nuclei through a diffusion layer of stagnant film having some concentration gradient. For diffusion controlled growth expression for the rate of growth is

$$\frac{dr}{dt} = \frac{D}{r} V_m (C_b - C_e) \quad (2.3)$$

where C_b is bulk concentration, C_e is equilibrium solubility of the solid and V_m is molar volume of the solid. An important aspect to note is that the inverse dependence of growth rate on particle size tends to narrow the size distribution after a while. Expression for the surface reaction controlled growth is

$$\frac{dr}{dt} = kV_m (C_b - C_e) \quad (2.4)$$

Expression (2.4) indicates that the growth rate is independent of particle size. This is the case when two dimensional growth of the nucleus by the deposited solute monomer is limited by the fast nucleation on the surface of the particle. This growth mechanism is called polynuclear-layer growth. But the two dimensional growth of the nucleus is considered to be extremely rapid compared to the two dimensional nucleation at early stages of the growth and the whole surface of the particle will be covered by a new solid layer initiated by single nucleus. This mechanism of the growth is called mononuclear-layer growth. In this case growth rate is proportional to the surface area of particle and is given by^[8]

$$\frac{dr}{dt} = kV_m r^2 (C_b - C_e) \quad (2.5)$$

Turkevich et al.^[5] experimentally found that the formation of gold colloids from its precursors HAuCl_4 and sodium citrate follows exponential growth mechanism as given by the following expression.

$$\frac{dr}{dt} = kr \quad (2.6)$$

where k is constant. Another extreme case is when the growth of nuclei is limited by the supply of monomers by chemical reaction between precursors. In this case growth rate is controlled by the reaction rate.

2.4 Literature survey

Formation of gold nanoparticles by chemical reduction method involves reduction of metal salt [typically gold chloride] with reducing agent in the presence of

a stabilizer. Schematic representation of formation of nanoparticles is shown in figure 2. In some cases the reducing agent can act as both reducing and stabilizing agent; so, no additional stabilizer is required. Literature survey indicates that the same method is applicable to form various metal nanoparticles^[9]. Several groups have reported on the kinetics of formation of nanoparticles by reactive crystallization. Overview of these reports is given below.

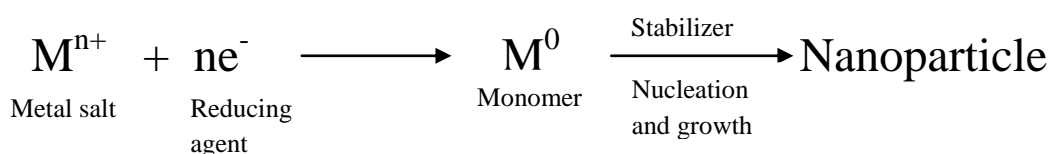


Fig. 2.2 Schematic illustrating the general principle of nanoparticle synthesis by chemical reduction method

Turkevich et al.^[6] first reported the kinetics of nucleation and growth during the synthesis of gold nanoparticles for citrate method. Sodium citrate and hydroxylamine hydrochloride were used as reducing agents of auric ion, but sodium citrate was found to act as both a nucleating and growth agent, while hydroxylamine hydrochloride functioned only as a growth agent that helped in determining number of nuclei. The general nature of the nucleation curve (number of nuclei per unit volume vs time) was characteristic of an autocatalytic reaction. Induction time was found to increase with increase in dilution of chloroauric acid and independent of citrate concentration. Final particle size was increasing for both with increase in dilution of chloroauric acid and decrease in concentration of citrate. The mechanism of growth was logarithmic.

Andreescu et al.^[10] reported variation of induction time with concentration of the chloroauric acid and pH of the chloroauric acid solution for formation of gold nanoparticles by reducing chloroauric acid (HAuCl₄) with iso-ascorbic acid. Induction period was found to decrease as the concentration of the gold salt increased. The mean size of the nanoparticles increased with an increase in the concentration of HAuCl₄ and this was attributed to coagulation of the nanoparticles. As pH increases induction time decreases till pH 4 and then increases. This was attributed to the pH dependent reactivity of gold precursor.

Abecasis et al.^[11] studied kinetics of gold nanoparticle formation by reduction of the gold salt in toluene with the borohydride salt (BH_4^-) in the presence of an excess of either decylamine or decanoic acid ligands. Stopped flow module (SFM-400) from Biologic coupled with diode array spectrophotometer, small and wide angle X-ray scattering (SAXS and WAXS) measurements were used to monitor the progress of the nanoparticle formation. The results show that in the case of acid ligand the nucleation takes place slowly and nucleation, growth regimes could be identified. But in the case of amine ligand nucleation occurred very rapidly and there was no growth phase. Time evolution of absorbance with time at 400 nm indicated that nanoparticles also contributing to the variation of the signal after some extent of reaction which was contradicting to the assumption of kinetic studies by traditional band assignment approach. This indicates the need of new analysis methods for analysing UV-Vis spectroscopic data for the better understanding of the kinetics of metal salt reduction and nanoparticle formation. SAXS results show that the mechanism of the growth was surface reaction controlled in the case of acid ligand.

Salvati R et al.^[12] studied kinetics of formation of gold nanoparticles by alcoholic reduction of the Au (III) ions, in the presence of a polymeric stabilizer while monitoring the formation of the nanoparticles by online optical spectroscopy. UV-Vis spectrum was recorded at various times from the start of the reaction. The recorded spectra were mainly attributed to three factors: 1). Absorption due to Au^{3+} ions, 2). $5d \rightarrow 6sp$ inter band transitions of gold atoms, and 3). Surface plasmon absorption band of gold clusters. Contributions from each of these factors for the spectrum were deconvoluted using the corresponding Lorentzian functions. Cubic root of the absorbance of surface plasmon resonance peak ($\sim d$) was plotted against time and a linear trend was found for temperatures more than $70^\circ C$, indicating that the growth mechanism is surface reaction controlled according to expression (2.8). An inherent assumption was that the nucleation rate was very high and as a result nucleation and growth stages could be separated. At temperatures below $70^\circ C$, a S-shaped curve was observed and it was attributed to the continuous formation of new nuclei during growth.

Wang J et al.^[13] first introduced a chemometric approach for the analysis of the time resolved UV-Vis spectra obtained in nanoparticles formation and applied it to the in situ monitoring of the kinetics of metal ion reduction and nanoparticle formation. This method is based on the combination of net analyte signal (NAS) and principal component analysis (PCA) chemometric methods which take the entire UV-Vis spectrum into account and offers better interpretation of the metal salt reduction and nanoparticle formation than the traditional band assignment approach.

Hemmateenejad et al.^[14] applied another chemometric method named multivariate curve resolution–alternating least squares (MCR-ALS) in processing the overlapped spectrum obtained in nanoparticle formation. They applied this method for the UV-Vis spectra obtained during CdSe nanoparticles formation from its precursors CdO and Se. This approach also takes the entire UV-Vis spectrum into account and is capable of extracting both concentration profiles and pure spectrum of the components involved.

From this overview, it is keen that the mechanisms of nucleation and growth are not fully understood and in deconvoluting UV-Vis spectra obtained during nanoparticle formation data analysis plays a critical part.

2.5 References

- [1]. Mersmann A (2001) Crystallization technology handbook. Marcel Dekker.
- [2]. La Mer V K (1952) Nucleation in phase transitions. Industrial and Engineering Chemistry 44:1270-1277.
- [3]. Mullin J W (2001) Crystallization. Butter Worth Heinemann.
- [4]. Chakraborty J (2008) Modeling and simulation frameworks for synthesis of nanoparticles. PhD Thesis, Indian Institute of Science.
- [5]. Nancollas G H and Purdie N (1964) The kinetics of crystal growth. Quarterly Reviews: 1-20.

- [6]. Turkevich J, Stevenson P C and Hillier J (1951) A study of the nucleation and growth processes in the synthesis of colloidal gold. *Faraday Society* 11:55-75.
- [7]. Kumar S, Gandhi K S, Kumar R (2007) Modeling of formation of gold nanoparticles by citrate method. *Industrial Engineering Chemistry and Research* 46:3128-3136.
- [8]. Sugimoto T (2001) *Monodispersed particles*. Elsevier.
- [9]. Gunter S (2004) *Nanoparticles from theory to application*. Wiley-VCH Verlag Gmbh & Corporation.
- [10]. Andreescu D, Sau T K, Goia D (2006) Stabilizer-free nanosized gold sols. *Journal of Colloidal and Interface Science* 298:742-751.
- [11]. Abecasis B, Testard F, Spalla O (2007) Probing in situ the nucleation and growth of gold nanoparticles by small angle X-ray scattering. *Nano Letters* 7(6): 1723-1727.
- [12]. Salvati R, Longo A, Carotenuto G (2004) Online monitoring of Au nanoparticles formation by optical spectroscopy. *The European Physical Journal B* 41 :43-48.
- [13]. Wang J, Boelens H F M, Rothenberg G (2004) In situ spectroscopic analysis of nanocluster formation. *Journal of Chemical Physics and Physical Chemistry* 5:93-98.
- [14]. Hemmateenejad B and Nezhad H R M (2008) Investigating the shape evolution mechanism of CdSe quantum dots by chemometrics analysis of spectroscopic data. *Journal of Physical Chemistry* 112: 18321-18324.

Chapter 3

Chemometric Methods for Spectroscopic Data Analysis in Nanoparticle Formation

UV-Vis spectroscopy is commonly used to study kinetics of metal nanoparticle formation. In gold nanoparticle formation, gold salt and gold nanoparticles have specific absorbance peaks at particular wavelengths as shown in figure 3.1. A common approach to estimate the concentration of gold salt and nanoparticles is to monitor the variation of absorbance at the corresponding wavelength peaks (univariate or uni-wavelength method). Typically, the absorbance corresponding to gold salt peak should continuously decrease with time, while the absorbance corresponding to gold nanoparticles should continuously increase. In a recent report^[1], it was found that the absorbance at gold salt peak increases after some time period. This is due to contribution of gold nanoparticles at the gold salt peak wavelength after some extent of reaction. So, the deconvolution of the composite signal into contributions from individual species is not feasible using univariate or band assignment approaches.

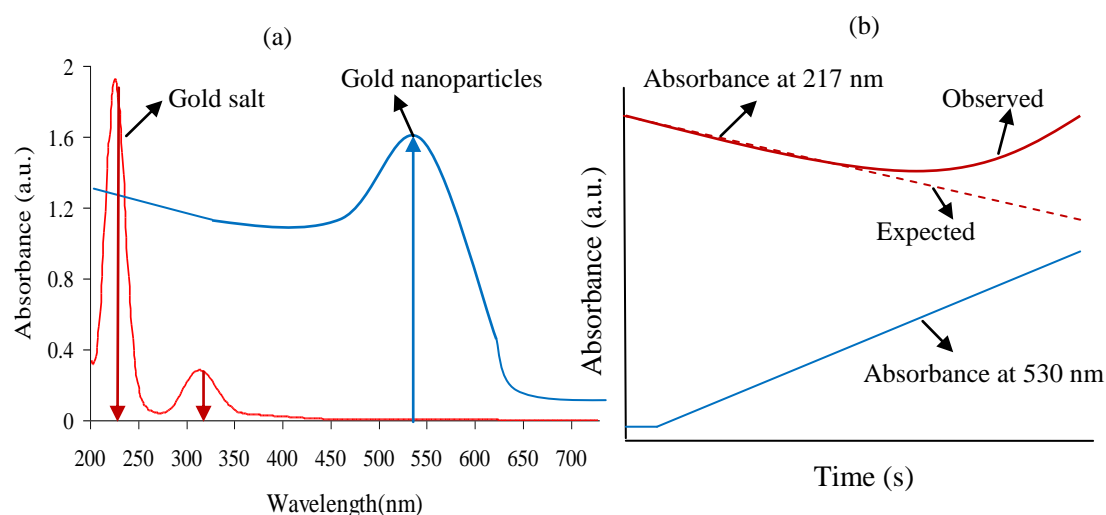


Fig. 3.1 (a) Schematic representation of the spectroscopic peaks corresponding to the gold salt and gold nanoparticles. (b). Time variation of the absorbance at wavelengths corresponding gold salt and gold nanoparticles peak position.

To understand kinetics of gold nanoparticles formation completely, it is necessary to know variation of the concentration of gold salt during nanoparticles formation. Application of chemometric methods on UV-Vis spectroscopic data is one way to get necessary information regarding kinetics of metal salt reduction and nanoparticles formation^[2,3]. These methods relate measurements made on a system or a process to the state of the system through application of mathematical or statistical methods^[4]. Basic assumption in all chemometric methods is that the Beer Lambert's law and superposition theorem are applicable for all components present in system^[5].

Chemometric methods operate over entire wavelength range (multivariate or multi-wavelength methods) and convey an insight about evolution of the various species with respect to time. Till date, two types of chemometric methods have been used in literature to analyse nanoparticle formation. They are: 1). Net Analyte Signal (NAS) and Principal Component Analysis (PCA) 2). Multivariate Curve Resolution-Alternating Least Squares (MCR-ALS) method. The objective of this chapter is to present a brief background about MCR-ALS method and demonstrate its capabilities by analysing spectra obtained during gold nanoparticle formation by citrate reduction at 50°C.

3.1 Net analyte signal (NAS) and principal component analysis (PCA)

Net analyte signal (NAS) of a component is defined as the part of the reaction spectrum which is orthogonal to the spectra of the other components (interferents)^[6]. In the case of formation of nanoparticles from its precursors, interfering components are solvent, reducing agent and stabilizer. Typically, the variation of the spectrum due to consumption of the reducing agent in the reaction is neglected, as it is taken in excess.

In the case of nanoparticle formation both the concentration of metal ions and nanoparticles will change as reaction progresses. Core reaction spectrum at any time is a combination of net analyte signal of metal ions and nanoparticles. It is calculated by projection of the reaction spectrum on the interferent space. NAS of the metal ions at start of reaction with respect to solvent, stabilizer and reducing agent is calculated using separately measured spectra of mixtures that contain only latter compounds (i.e.

spectrum at start of the reaction)^[3]. From this vector, the NAS vector of metal ions at any time can be obtained by vectorial projection of the reaction spectrum in the direction of the metal ion NAS vector at the start of the reaction (reaction spectrum without nanoparticles). From the core reaction spectra, subtract metal ions contribution to obtain remaining signal. The remaining signal is analysed using principal component analysis (PCA) to find out number of active spectral components that are responsible for variation in remaining signal^[3].

NAS and PCA analysis gives only variation of the concentration of various evolving species with respect to time. MCR-ALS gives both concentration profiles and pure spectra of the all evolving components. Other problem with NAS is that NAS of each and every component should be calibrated to concentration. Availability of standard solutions for calibration is another problem with NAS and PCA. A brief description about MCR-ALS is presented below.

3.2 Multivariate curve resolution-alternating least squares method (MCR-ALS)

MCR-ALS is an iterative optimization process which gives pure component concentration profiles and spectra of individual components that are evolved in the reaction. Decomposition of the data matrix A ($n \times m$) into concentration matrix C ($n \times k$) and pure spectra matrix S^T ($k \times m$) is shown in figure 3.2. Mathematical view point all curve resolution methods are subjected to ambiguities i.e. decomposition of the data matrix is not unique^[5].

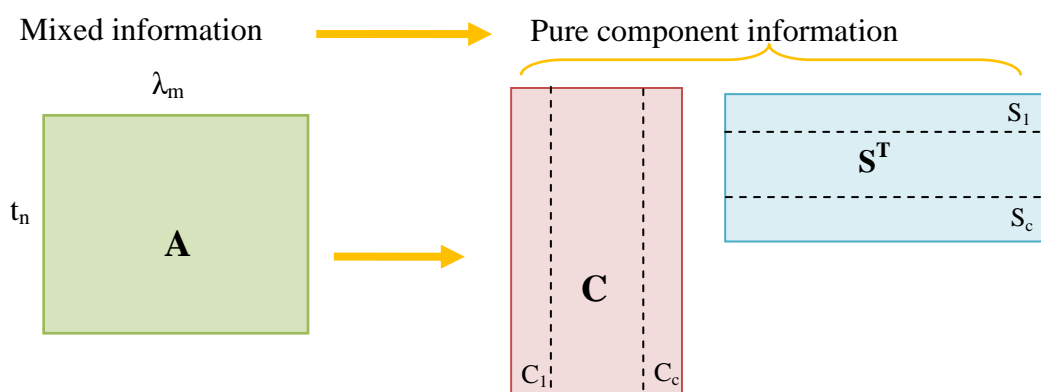


Fig. 3.2 Decomposition of data matrix D into concentration matrix C and pure component spectra matrix S^T ^[5].

3.2.1 Ambiguities associated with curve resolution

Decomposition of the data matrix A can be achieved by using component profiles that are different in shape. This is called rotational ambiguity.

$$\text{Expression for the real decomposition: } A_{n \times m} = C_{n \times k} S_{m \times k}^T \quad (3.1)$$

$$\text{This expression can be transformed into: } A = (CR)(R^{-1}S^T) \quad (3.2)$$

$$A = C'S'^T \quad (3.3)$$

where R is any non-singular matrix, C' and S'^T are transformed concentration and spectra matrices. We can construct infinite non-singular matrices, so, data matrix A can be decomposed in infinite ways.

Data matrix A can also be decomposed using component profiles that are different in intensity. This is called intensity ambiguity.

$$A = CS^T = \sum_{i=1}^n \left(\frac{1}{k_i} C_i \right) (k_i S_i^T) \quad (3.4)$$

where k_i is scalar and n is number of components.

These ambiguities can be eliminated by using component information obtained by analysing data matrix and by forcing all concentration and spectra profiles to follow certain constraints^[5]. A detail of implementation of MCR-ALS is discussed in coming sections.

MCR-ALS uses principal component analysis (PCA) and evolving factor analysis (EFA) methods as starting points. PCA gives information about the number of factors that are responsible for the variation in data. EFA builds initial estimates for the concentrations profiles of all significant components and these concentration profiles are used as starting point for iterative optimization process subjected to constraints^[5]. A brief description about PCA and EFA are presented below.

3.2.2 Principal component analysis (PCA)

Principal component analysis is a process of eliminating random noise associated with the principal components thereby reducing the dimensionality of the

complex data set and minimizing the effects of measurement error^[5]. If A is a data matrix of size $n \times m$, then, application of the PCA on the data matrix gives the following expression

$$A_{n \times m} = T_{n \times k} V_{m \times k}^T + \epsilon \quad (3.5)$$

where V is called loadings or eigenvector matrix and it forms row basis vectors of A by linear combination of its column vectors. T is called scores matrix and it forms column basis vectors of A by linear combination of its column vectors. n is number of objects (time points), m is number of variables (wavelengths points), k is number of independent components and ϵ is unexplained variance of the data matrix.

For each independent source of variation in the data, a single principal component is expected in PCA. The first column in loadings and score matrix corresponds to the first principal component. The first eigenvector in loadings matrix corresponds to the largest eigenvalue, so, PC1 explains largest variation in the data matrix. Similarly, the second column in the loadings and score matrix corresponds to the PC2 and it explains the next largest variation in the data remaining after PC1. The data matrix A can be written as the sum of all principal component matrices plus unexplained variance of the data matrix^[5].

$$A = t_1 v_1^T + t_2 v_2^T + t_3 v_3^T + \dots + t_k v_k^T + \epsilon \quad (3.6)$$

The first term in the above expression gives the variance explained by PC1. Singular value decomposition (SVD) model is commonly used to build data sets i.e. scores and loadings matrices of PCA. The variance explained by the j^{th} principal component is defined as the ratio of the j^{th} eigenvalue to the total variance in the data matrix^[5].

$$\% \text{ var by } j^{\text{th}} \text{ PC} = \frac{\lambda_j}{\sum_{i=1}^k \lambda_i} \quad (3.7)$$

The cumulative variance explained by principal components 1 to j is given by the following expression^[5]

$$\text{cum \% var from } 1-j = \frac{\sum_{i=1}^j \lambda_i}{\sum_{i=1}^k \lambda_i} \quad (3.8)$$

3.2.3 Evolving factor analysis (EFA)

EFA is useful to understand the evolution of various species during progression of a reaction. It performs PCA on sub matrices of gradually increasing in size, starting from a matrix having two rows and adding one row at each subsequent step, until the final row. By applying PCA from top to bottom (forward EFA) and bottom to top (backward EFA), the emergence and decay of various species can be understood^[5].

Forward EFA plot is produced by plotting log of eigenvalues (e.v.) obtained by performing PCA on sub matrices expanding in forward direction. Similarly, backward EFA plot is produced by plotting log of e.v. obtained by performing PCA on sub matrices expanding in backward direction. Eigenvalues in forward and backward directions give emergence and decay of concentration of various constituents. For a system with n significant components, estimation of concentration profile of first component can be obtained by combining the curve representing the first e.v. curve of forward EFA plot and combining the curve representing n^{th} e.v. curve of backward EFA plot. Estimation of concentration profile of second component can be obtained by combining 2^{nd} e.v. curve of forward EFA plot and $n-1^{\text{th}}$ e.v. curve in backward EFA plot^[5].

3.2.4 Constraints in MCR-ALS

Constraint is defined as a mathematical or chemical property that is systematically fulfilled by whole system. The constraints for the application of MCR-ALS method to nanoparticles formation are non-negativity constraints for both concentration profiles and pure spectra, unimodality constraints for concentration profiles and normalization constraint on spectra profiles. If we know the stoichiometry of the metal salt reduction and nanoparticles formation, we can also apply closure constraints and that will give us the absolute concentration of all

evolving components quantitatively^[5]. The mathematical model expressions involved are described the following.

3.2.5 Objective function in MCR-ALS

The objective function that is optimized using alternating least square (ALS) method is the following

$$\text{Minimize } \|D_{\text{PCA}} - C_t S_t^T\| \quad (3.9)$$

Subjected to nonnegitivity constraint on both C and S,
 unimodality constraint on C,
 normalization constraint on S.

where D_{PCA} (n x m) is data matrix with selected number of principal components obtained from PCA, C is concentration matrix and S is pure component spectra matrix. Variables to be optimized in objective function are C and S; so, minimize the objective function with respect to C and S. After least square optimization the following expressions for C and S^T can be obtained.

$$C_{t+1} = D_{\text{PCA}} S_t (S_t^T S_t)^{-1} \quad (3.10)$$

$$\text{If } S \text{ is not full rank matrix, then: } C_{t+1} = D_{\text{PCA}} S_t^+ \quad (3.11)$$

where S_t^+ is pseudoinverse of S_t .

$$\text{Expression for } S \text{ is: } S_{t+1}^T = (C_t^T C_t)^{-1} C_t^T D_{\text{PCA}} \quad (3.12)$$

$$\text{If } C \text{ is not full rank matrix, then: } S_{t+1}^T = C_t^+ D_{\text{PCA}} \quad (3.13)$$

Convergence criterion for the MCR-ALS is norm of the residual matrix (i.e. D_{PCA} with selected number of components – $C^* S^T$ estimated by alternating least squares method) is equal to or less than some threshold value^[5].

3.2.6 Steps in MCR-ALS method

The various steps involved in analysing absorbance data in accord with MCR-ALS are listed below.

1. Determine number of principal components in data matrix (D) using PCA.
2. Calculate an initial estimate for C matrix using EFA.
3. Using an estimate for C, calculate S^T using least squares formula under appropriately chosen constraints.
4. Using S^T , calculate C using least squares formula under appropriately chosen constraints.
5. From the product of C and S^T found in the above iterative steps, calculate norm of the residual matrix and check convergence criteria.
6. Repeat steps 3, 4 and 5 until convergence is achieved.

3.3 Validation of the MCR-ALS method

MCR-ALS method was validated by performing analysis on a known 2 component evolving spectroscopic data. The data was generated by scale down and scale up of the gold the salt and gold nanoparticles pure spectra linearly. The generated evolving spectroscopic data is shown in figure 3.3.

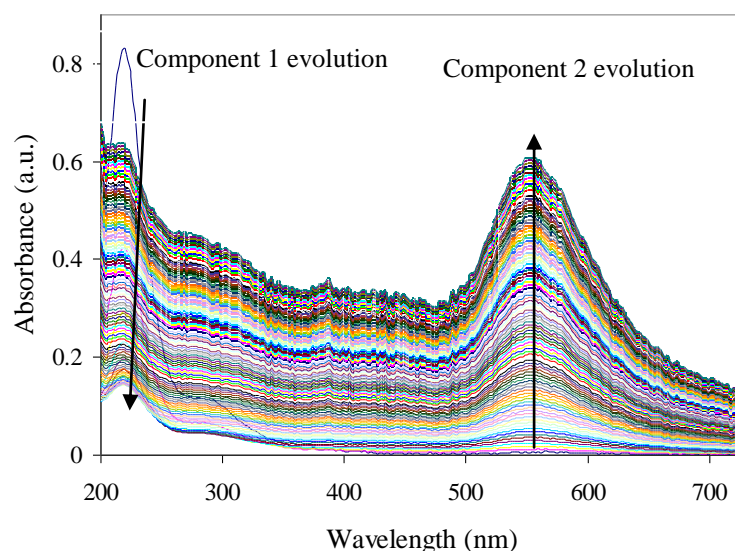


Fig. 3.3 Evolution of the generated UV-Vis spectroscopic data. Concentration of gold salt decreases and concentration of nanoparticles increases linearly.

The MCR-ALS method was implemented in MATLAB environment (version 7.3). The generated evolving spectroscopic data was analysed using MCR-ALS. Analysis was carried using user friendly graphical interface developed by Tauler group^[6]. The code for EFA was taken from website^[7] and code for PCA was developed in house.

The principal component analyses showed that 2 components are sufficient to explain 99.9 % of the variation in the data set. An estimate for the initial concentration matrix was obtained by performing evolving factor analysis. Inputs for the MCR – ALS program are data matrix, initial estimate for the concentration matrix and constraints. Non-negativity constraints for both concentration and spectra, unimodality constraints for concentration and normalization constraint on spectra matrix were applied during analysis. Normalised expected and theoretical pure spectra of component 1 and component 2 are shown in figure 3.4. Pure spectra of the components obtained from the analysis are matching well with the expected pure spectra.

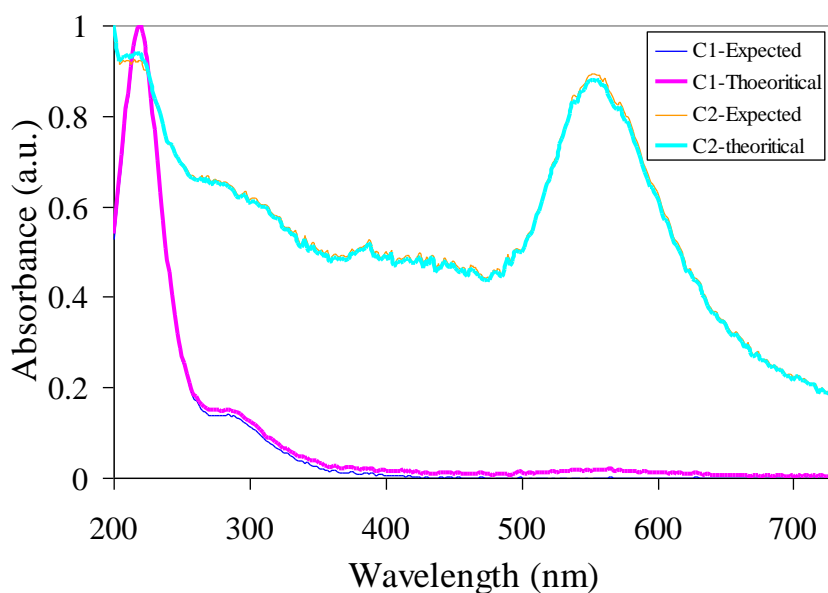


Fig. 3.4 Normalised expected and theoretical spectra of components.

Expected and theoretical concentration profiles of component 1 and component 2 are shown in figure 3.5 and 3.6 respectively. The concentration profiles of component 1 are deviating from expected concentration profiles starting from 30 s onwards. The reason for the deviation is the following. According to MCR-ALS all components should evolve and component of each and every species should reach zero at particular time. The generated spectroscopic data is first order and for first order system it requires longer times to reach zero concentration. The concentration profiles of component 2 also deviating from expected profiles at starting times. The reason for this is the same as component 1.

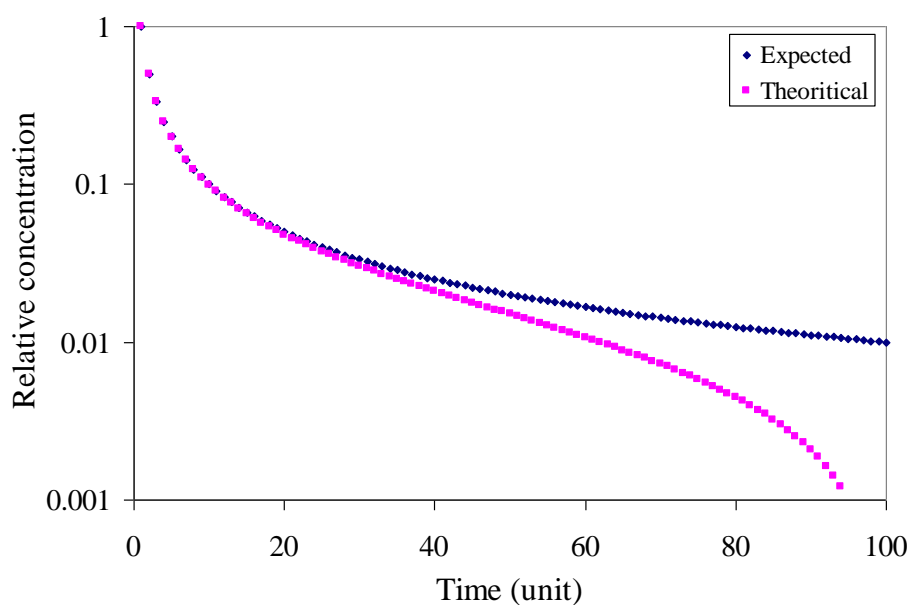


Fig. 3.5 Normalised expected and theoretical concentration profiles of component 1.

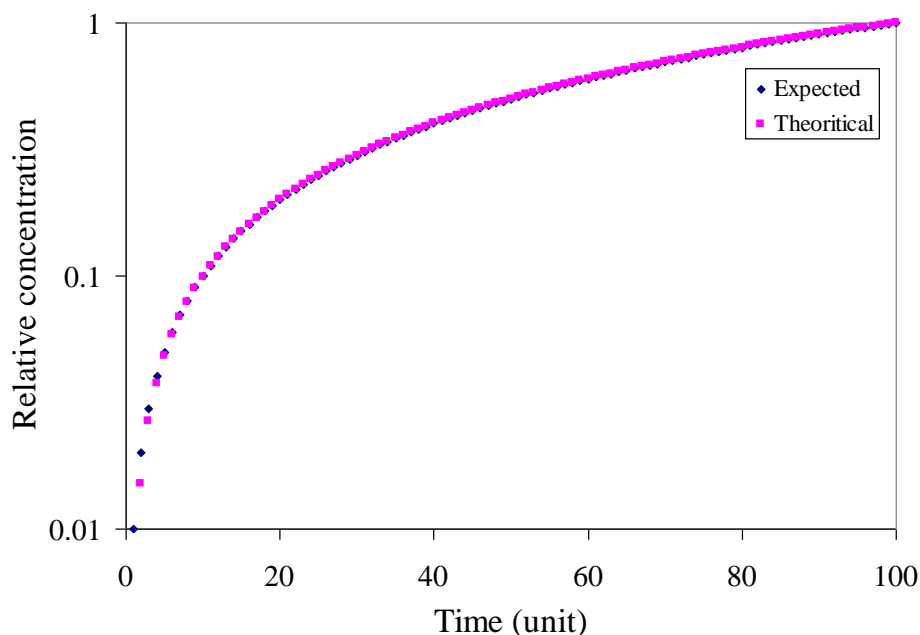


Fig. 3.6 Normalised expected and theoretical concentration profiles of component 2.

3.4 Analysis of the data obtained during gold nanoparticle formation by citrate method

The data obtained during gold nanoparticles formation by citrate method was analysed using MCR-ALS. Chloroauric acid (HAuCl_4) and sodium citrate at reaction temperature of 50°C were used as precursors for nanoparticle synthesis. Stopped flow module (SFM-400) coupled with high UV-Vis light source and diode array spectrometer were used to study the kinetics of nanoparticle formation. UV-Vis spectrum in wavelength range 260 -730 nm was taken at variable time steps starting from time of mixing to completion of nanoparticle formation. The 3D evolution of the UV-Vis spectrum is shown in figure 3.7.

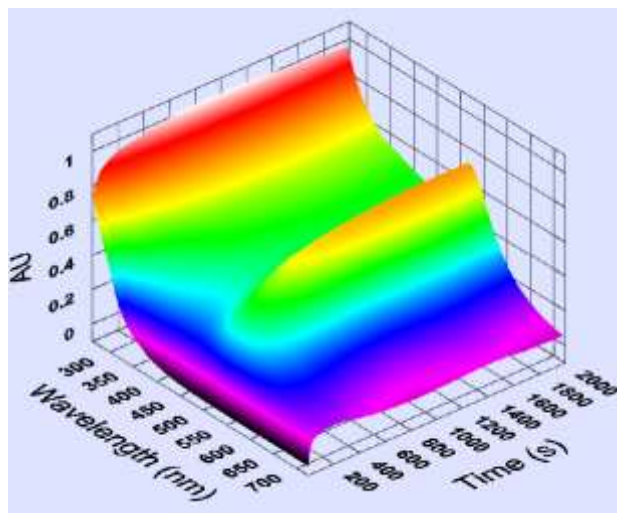


Fig. 3.7 Evolution of the UV-Vis spectrum during the formation of gold nanoparticles by citrate method.

3.5 Results obtained with MCR-ALS method

MCR-ALS analysis was carried using user friendly graphical interface developed by Tauler group^[6]. The code for EFA was taken from website^[7] and code for PCA was developed in house. Results of the analysis method are discussed below. PCA was carried out on original data matrix to find out number of UV-Vis active components that are responsible for the variation of data. Result of the PCA is summarized in table 3.1. This data indicates that three principal components are enough to explain around 99.9 % systematic effects.

Component	E.V.	CPV
1	94993	98.5
2	1163	99.7
3	197	99.9
4	6	99.9
5	2	99.9

Table 3.1 Results of the PCA on the spectroscopic data obtained for the nanoparticles formation by citrate method. E.V.: Eigenvalue; CPV: Cumulative percentage variance

Normalised pure spectra and concentration profiles obtained from MCR-ALS analysis are shown in figure 3.8 and 3.9 respectively. The component 1 spectrum is similar to gold salt UV-Vis spectrum and its concentration decreases with time. So, we can assign component 1 to gold salt. Component 2 has absorbance peak at around 580 nm and its concentration is zero at initial, final times and maximum at intermediate times. This indicates that the component 2 is big intermediate. Component 3 has absorbance peak at around 530 nm and its concentration profile resembles sigmoidal curve which is a characteristic of nanoparticle formation. So, we can assign component 3 to nanoparticle.

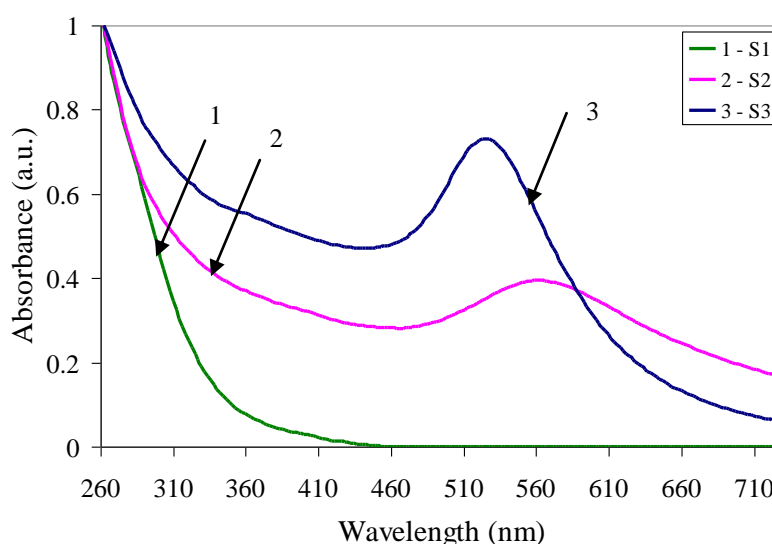


Fig. 3.8 Normalised pure spectra of the individual components obtained from MCR-ALS method. S1: Spectra of the intermediate; S2: spectra of the intermediate; S3: spectra of the nanoparticles.

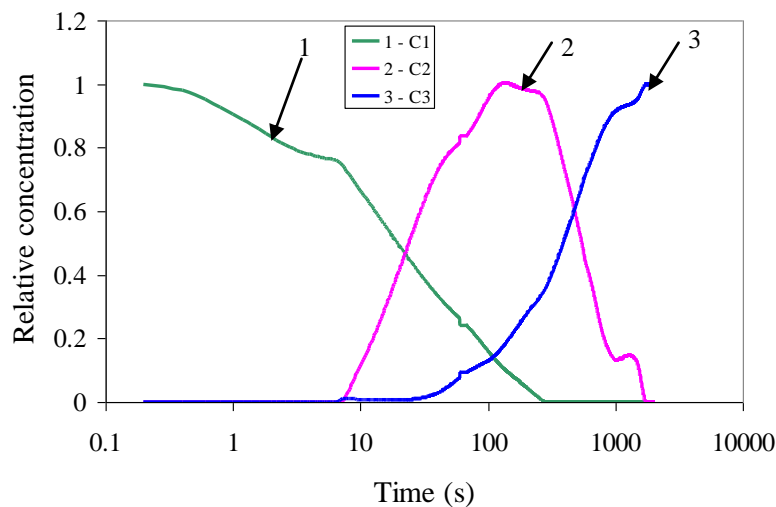


Fig. 3.9 Optimized concentration profiles of evolving components; C1: Concentration profile for gold salt; C2: Concentration profile for intermediate; C3: concentration profile for nanoparticles

The results obtained from MCR-ALS are in concord with the TEM images taken during nanoparticle formation^[8]. TEM images showed that a big intermediate form at early stages and this will brake down into smaller spherical nanoparticles in final stages. TEM images of samples at various stages are shown in figure 3.10. Using MCR-ALS method we were able to get the same information which is obtained sophisticated instrument like TEM.

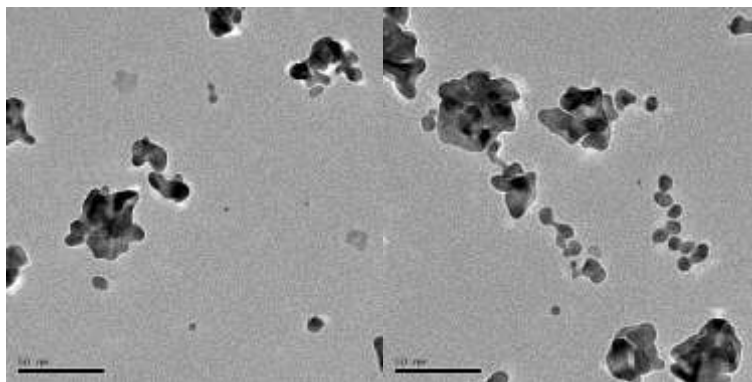


Fig. 3.10 TEM images of the samples collected at various stages of formation of gold nanoparticles by citrate method. First a big intermediate will form and this will break down into smaller nanoparticles at later stages^[8].

3.6 Summary

MCR-ALS method was implemented and the data obtained during gold nanoparticle formation by citrate method was analysed using this method. MCR-ALS method gives concentration profiles and pure spectra of all evolving components. The results obtained from analysis are in agreement with the TEM images taken during nanoparticle formation.

3.7 References

- [1]. Abecasis B, Testard F, Spalla O (2007) Probing in situ the nucleation and growth of gold nanoparticles by small angle X-ray scattering. *Nano Letters* 7(6): 1723-1727.
- [2]. Bahram H and Reza H N (2008) Investigating the shape evolution of CdSe quantum dots by chemometrics analysis of spectrophotometric data. *Journal of Physical Chemistry C* 112 (47) : 18321–18324.
- [3]. Wang J, Boelens H F M, Rothenberg G (2004) In situ spectroscopic analysis of nanocluster formation. *Journal of Chemical Physics and Physical Chemistry* 5:93-98.
- [4]. <http://en.wikipedia.org/wiki/Chemometrics> accessed on 20/12/08.
- [5]. Gemperline P. (2006) Practical guide to chemometrics. Taylor & Francis Group.
- [6]. Lorber A. (1986) Error propagation and figures of merit for quantification by solving matrix equations. *American Chemical Society* 58(6): 1167-1172.
- [7]. <http://www.ub.edu/mcr/welcome.html> accessed on 10/12/08.
- [8]. TEM images were taken from Sankar Kalidas (phD scholar, Dept. of Chemical Engg., IISc).

Chapter 4

Kinetics of gold nanoparticle formation

The precursors used for formation of gold nanoparticles are quite reactive; so, nanoparticle formation occurs on a time scale of seconds. Therefore, to study the kinetics, a fast mixing device that can mix reagents in time scale of milliseconds is needed. To perform this task, we used a stopped flow module (SFM) coupled with diode array spectrophotometer (refer appendix A). The 3D spectra (absorbance-wavelength-time) obtained from experiments was analysed using MCR-ALS method. The objective of this chapter is to understand kinetics of gold nanoparticles formation by redox reactions.

4.1 Feasibility studies

Anusha^[1] studied kinetics of gold nanoparticle formation using univariate methods by monitoring variation of the absorbance at 530 nm for the reduction of gold chloride by tannic acid. Initially, our plan was to study kinetics of gold salt reduction for this protocol. So, we carried out feasibility studies for using multivariate analysis tools. During experiments, Anusha^[1] maintained gold salt and tannic acid solutions pH at 3.2 and 7.7 respectively. In this protocol, after mixing the two reagent precursors the reaction mixture pH varies during initial stage of nanoparticle formation. If UV-Vis spectrum of the gold salt and tannic acid varies significantly with pH, then, multivariate analysis will assign such variation to separate species. So, experiments were performed to find out variation of the UV-Vis spectrum of HAuCl_4 and tannic acid with pH.

Variation of UV-Vis spectrum of 0.05 mM chloroauric acid with pH is shown in figure 4.1. It has two peaks and both of these are due to metal-ligand charge transitions^[2]. Intensity of both peaks decreases with increase in pH and the peak at 312 nm disappears at a pH >2 . UV-Vis spectra at pH 3-10 show that the absorbance at around 205 nm is almost constant irrespective of the pH of solution (isosbestic point). To confirm this point, UV-Vis spectrum at various pH for half of the earlier concentration of HAuCl_4 (0.0025 mM) was taken and is shown in figure 4.2. These

spectra also show that the absorbance at 205 nm is independent of pH and if we account the contribution to absorbance due to NaOH and HCl, absorbance at 205 nm

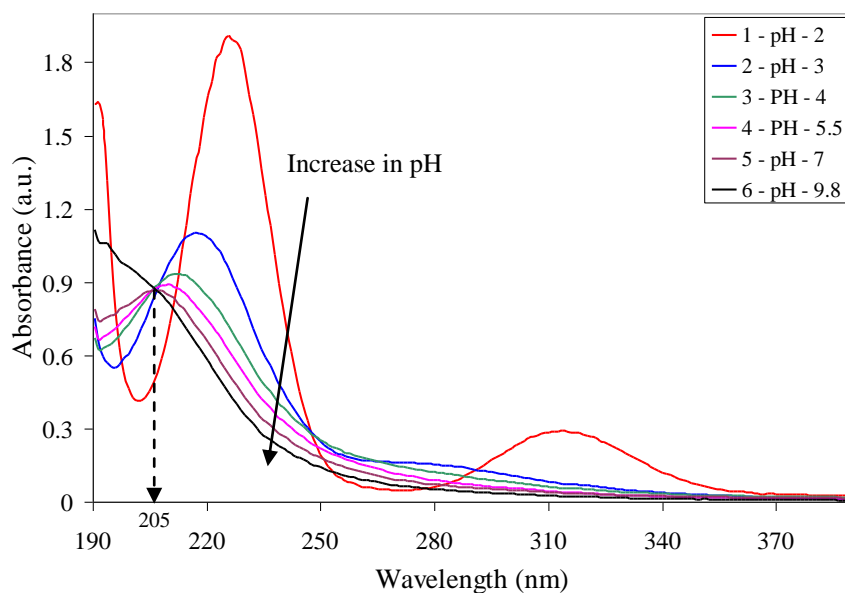


Fig. 4.1 Variation of the UV-Vis spectrum of 0.05 mM chloroauric acid solution with pH. It has two peaks at pH 2; as pH increases intensity of absorbance at both peaks decreases and at pH >2 peak at 312 nm disappears. For pH>2, the absorbance at 205 nm is independent of pH (isosbestic point).

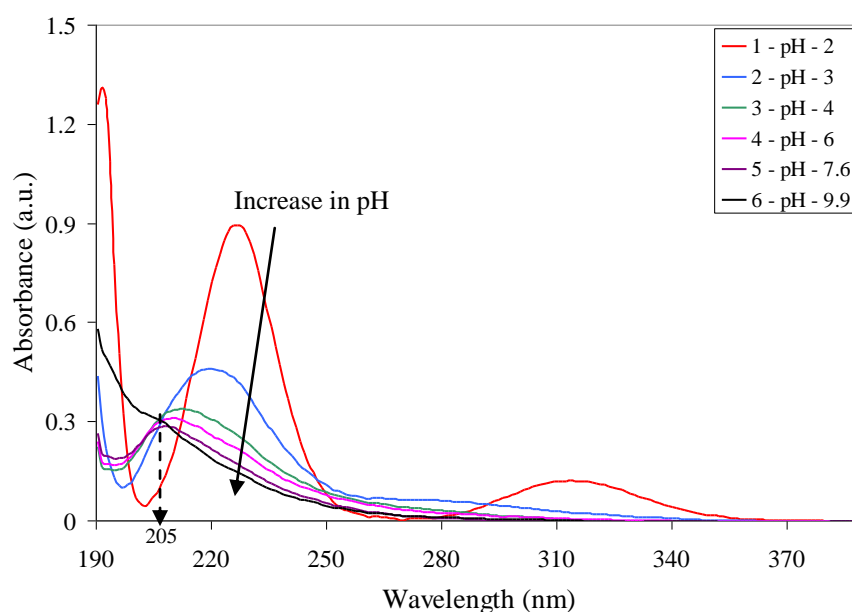


Fig. 4.2 Variation of the UV-Vis spectrum of 0.05 mM chloroauric acid solution with pH. It has two peaks at pH 2; as pH increases intensity of absorbance at both peaks decreases and at pH >2 peak at 312 nm disappears.

for 0.0025 mM concentration is almost half of the absorbance for 0.05 mM concentration. So, absorbance at isosbestic point can be used as a measure of chloroauric acid concentration.

UV-Vis spectrum of 5.9×10^{-3} mM concentration of tannic acid at various pH is shown in figure 4.3. The shape of UV-Vis spectrum is changing with pH. Tannic acid also exhibits two isosbestic points at 250 and 293 nm. However, the absorbance of tannic acid at 205 nm (isosbestic point of gold chloride) will be above the linear range of the instrument. So, it is not possible to study kinetics of gold salt reduction in SFM for tannic acid method.

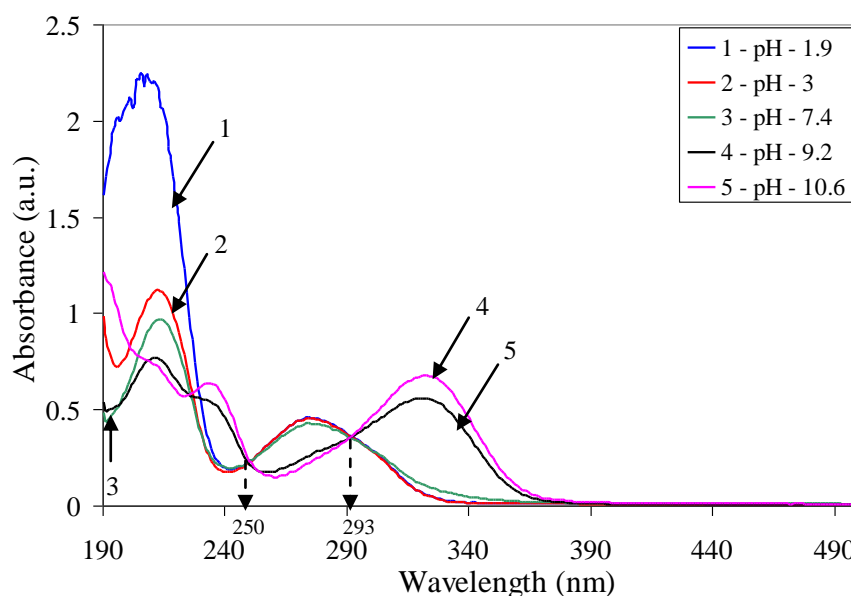


Fig. 4.3 Variation of the UV-Vis spectrum of 5.9×10^{-3} mM tannic acid with pH. The shape of the UV-Vis spectrum is completely changing with pH. Absorbance at 250 and 293 nm is independent of pH.

One other method that is most commonly used for gold nanoparticle synthesis is citrate method. Though, this protocol was developed in 50s, still, the mechanism of gold nanoparticle formation was not understood completely. For this protocol, we planned to study kinetics of gold salt reduction and nanoparticle formation at various molar ratios of sodium citrate to chloroauric acid, and effect of addition PVP stabilizer on reduction kinetics and final particle size. Reaction mixture pH at all molar ratios for both with and without PVP was maintained at around 3.2. Experiment

was performed to find out variation of the UV-Vis spectrum of citrate with pH and figure 4.4 shows this variation. UV-Vis spectrum of citrate is varying significantly with pH. If pH changes during reaction both gold salt and citrate will contribute to the variation in UV-Vis spectra. So, to study kinetics for citrate method we have to maintain gold salt and sodium citrate solutions at same pH.

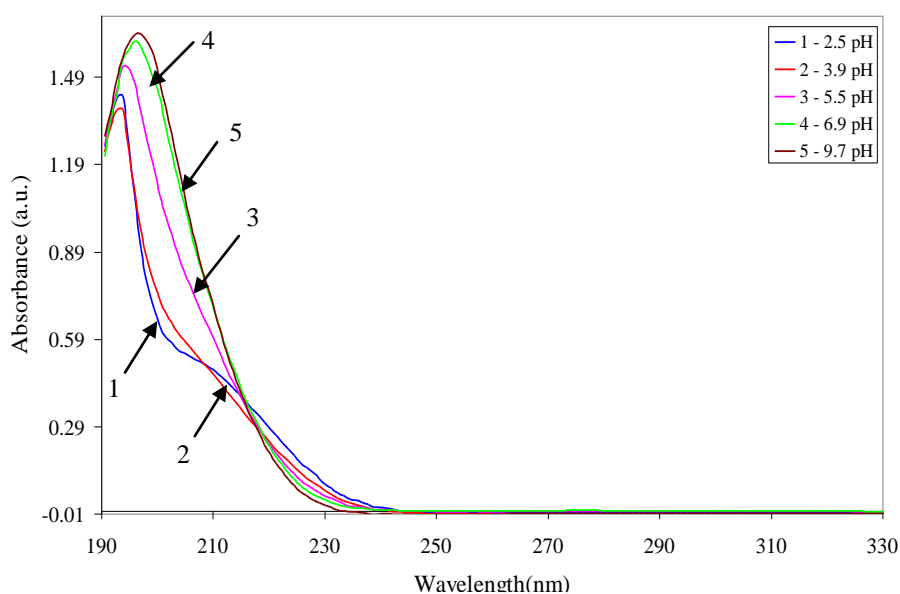


Fig. 4.4 Variation of the UV-Vis spectrum of 1.4 mM sodium citrate with pH. Absorbance contribution by citrate is decreasing with decrease of pH in UV range.

During kinetics studies of gold nanoparticle formation, it was observed that gold salt decomposes in presence of UV-Vis light. Variation of the UV-Vis spectrum of gold salt in presence of UV-Vis light was recorded. Figure 4.5 shows variation of the absorbance at 217 nm peak. Around 24 % of the HAuCl_4 is decomposing with in 150 s and after that decomposition is zero. Effect of UV light on decomposition was obtained by exposing the sample to only visible light. Absorption spectrum was recorded for each 3 minutes while sample was exposed to only visible light for 30 minutes (except during scan) and to both UV and Vis lights from 30 to 33 minutes. Variation of the absorbance at 217 nm is shown in figure 4.6. When sample is exposed to Vis light there is no significant change in absorbance and absorbance drops suddenly in the presence of UV and Vis lights. This clearly shows that UV light is only responsible for the decomposition of HAuCl_4 .

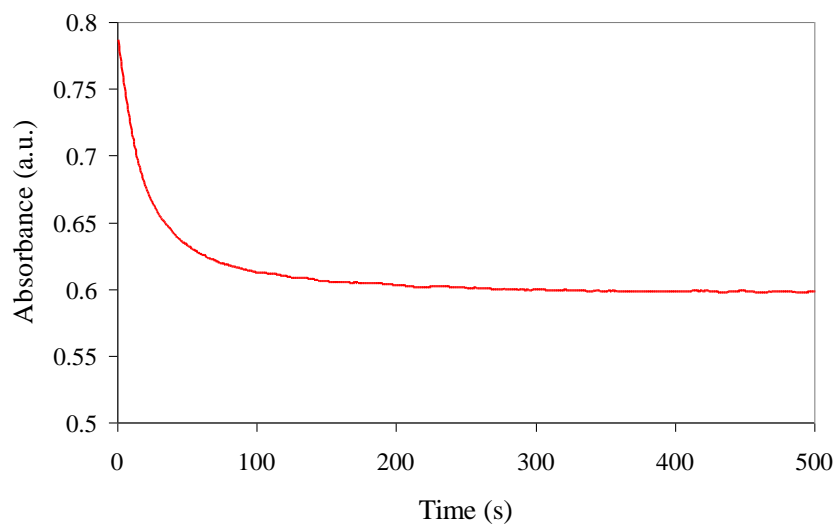


Fig. 4.5 Variation of the absorbance at 217 nm when 0.254 mM HAuCl_4 solution is exposed to UV-Vis light. Around 24 % of the gold salt is decomposed with in 150 s.

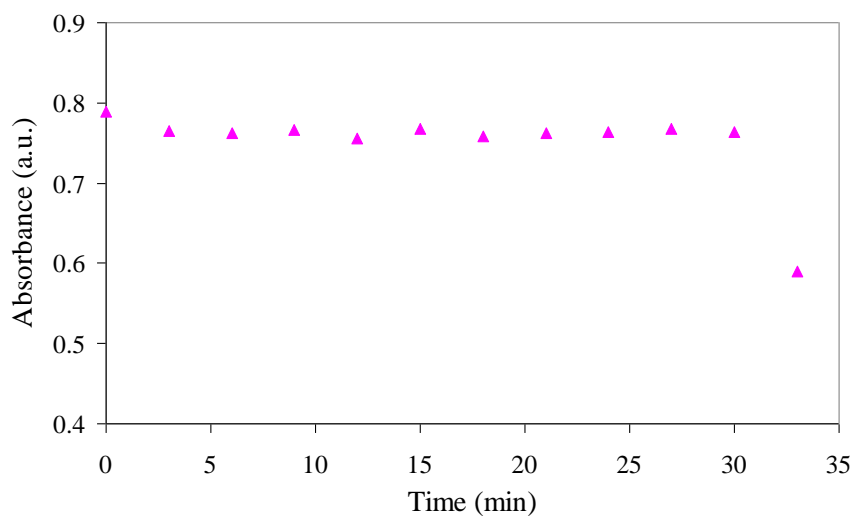


Fig. 4.6 Variation of the absorbance at 217 nm when 0.254 mM HAuCl_4 solution is exposed to only Vis light for 30 minutes and to both UV and Vis light from 30 to 33 minutes. Variation in presence of Vis light is negligible and absorbance drops suddenly in presence of UV and Vis lamps.

Other interesting thing about this decomposition is that the gold salt decomposition is reversible. Variation of the UV-Vis spectra of chloroauric acid in presence of UV and Vis light was taken for about 100 s and then, both UV and Vis lights was switched off for 15 minutes. After that, again variation of the UV-Vis spectra was recorded in the presence of UV and Vis light for about 100 s. As shown in figure 3.8 both variations are starting and ending at almost same points. Obviously, this indicates that the decomposition of gold salt is reversible.

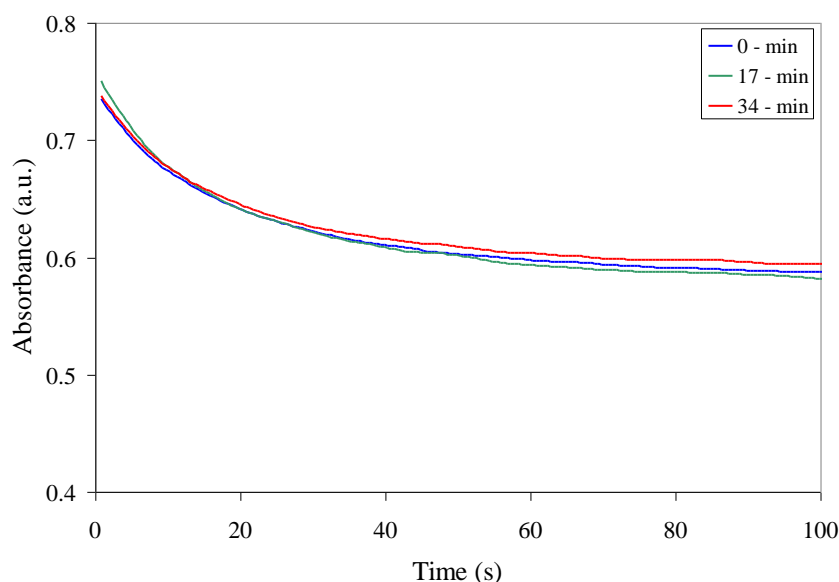


Fig. 4.7 Reversible decomposition of $\text{H[AuCl}_4\text{]}$ in presence of UV and Vis light. UV-Vis spectra were taken for 100 s by exposing sample to UV and Vis light and then, both lights were switch off for about 15 minutes. After that, again UV-Vis spectra were taken for 100 s by exposing sample to UV and Vis light.

It is not possible to study kinetics of nanoparticles formation without altering light source because the gold salt which is decomposed may affect the nucleation process. The UV-Vis light source that we were using has a shutter which can be controlled externally. Voltage required for opening and close of shutter was found out. Required voltage waveform as shown in figure 3.9 for light source shutter control was generated using keithley model 6221 AC and DC current source. Diode array shutter was set to open only during scan. A trigger signal was sent to keithley current

source when diode array shutter starts recording spectra. Diode array shutter wave form shape is shown in figure 4.8. When light source shutter is open for 220 ms (for

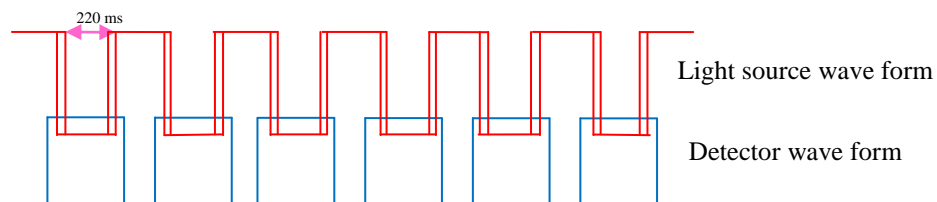


Fig. 4.8 Shape of voltage wave form to control UV-Vis light source shutter and Diode array shutter wave form.

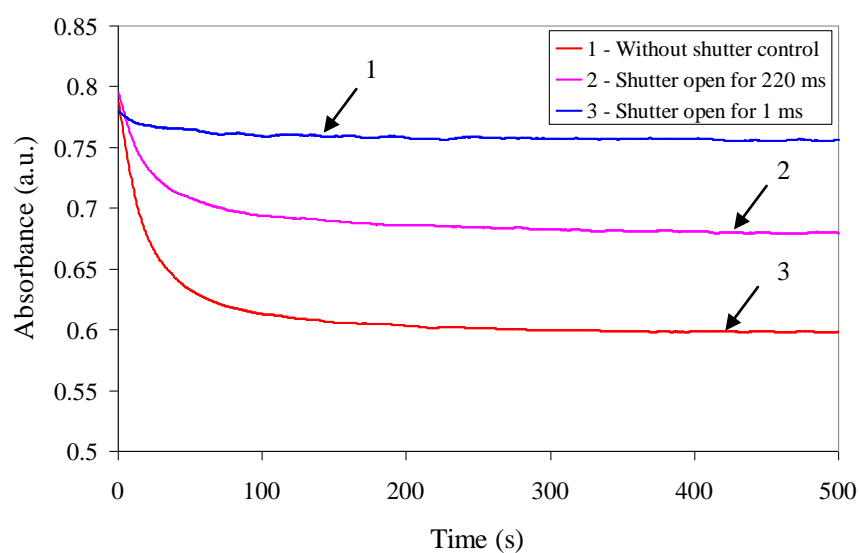


Fig. 4.9 Decomposition of $\text{H[AuCl}_4\text{]}$ with and without shutter control. Without shutter control decomposition is 24 % and with shutter control, for 220 ms shutter open decomposition is 14 % and for 1 ms open decomposition is 3 %.

each 0.5 s) decomposition of HAuCl_4 was around 14 %. By opening the light source shutter for about 1 ms, decomposition was reduced to 3%. Decomposition of HAuCl_4 with and without shutter control is shown in figure 4.9.

4.2 Kinetics of gold nanoparticles formation by citrate method

Synthesis of gold nanoparticles by citrate method was first reported by Turkevich et al. in 1951^[3]. Since, many people have studied this method and substantial amount of information about this method is available in literature. In this method citrate plays the following roles: 1). reduction of HAuCl_4 , 2). protection of nanoparticles from aggregation 3). pH control of reaction mixture^[4]. Turkevich et al. reported that as molar ratio of the citrate to chloroauric acid increases from 0.67 to 3.3 particle diameter changes from 24 nm to 14.5 nm^[3]. Frens also reported that as molar ratios of citrate to HAuCl_4 increases from 0.43 to 2.7 particle size changes from 147 nm to 16 nm^[5]. The particle size reported by Frens at lower molar ratios was different from Turkevich et al^[3,5]. Turkevich reported that as molar ratios increases the time required for completion of reaction increases^[3]. But, Frens reported opposite^[5].

Xiaohui Ji et al. reported that variation of particle size observed by Turkevich et al. and Frens are due to variation of the pH of reaction mixture as citrate act as pH mediator^[4]. They reported that at particular molar ratio particles with different size can be obtained by varying pH of reaction mixture^[4]. The time scales of reaction that Xiaohui Ji et al. reported were in agreement with Turkevich et al^[3,4]. Xiaohui Ji et al. reported kinetics of gold salt reduction at various molar ratios of citrate to chloroauric acid. In their studies pH of the reaction mixture was not controlled.

Kinetics of gold salt reduction and nanoparticles formation at variable molar ratios while maintaining reaction mixture at constant pH was not understood. In this chapter kinetics of gold salt reduction and nanoparticle formation, and final particle size at various molar ratios of citrate to chloroauric acid while maintaining reaction mixture pH at 3.2 is reported. Effect of addition of Poly Vinyl Pyrrolidone (PVP) on kinetics and final particle size were also reported. Stopped flow module (SFM) coupled with diode array spectrometer (refer appendix A) was used to gather UV-Vis

spectroscopic data at rapid rate. The 3D (wavelength-absorbance-time) spectroscopic data was analysed using MCR-ALS method discussed in chapter 3.

4.2.1 Materials used

Chloroauric acid ($\text{HAuCl}_4 \cdot 3\text{H}_2\text{O}$) from Acros, sodium citrate from Aldrich, Poly vinyl pyrrolidone (PVP) from Rolex laboratories and HCl from Sd Fine chemicals were used in experiments.

4.2.2 Experimental details

Temperature maintained in all experiments was around 60°C . During kinetic experiments, syringes S1, S2 and S3 were filled with 0.254 mM chloroauric acid and sodium citrate (concentration from 0.164 mM to 1.33 mM) respectively. Syringe S3 was filled with DI water and this DI water was used for background signal. Variation of the UV-Vis spectra was recorded from start of mixing of reagents to the completion of reaction with resolution of 1 s. By controlling shutter, sample was exposed to UV-Vis light only for 10 ms during each spectrum. To study effect of PVP on kinetics, PVP of 32 μM concentration was used. Reaction mixture pH maintained in all experiments was around 3.2.

4.3 Results and discussion

4.3.1 Kinetic studies

Kinetics of gold salt reduction and nanoparticle formation were studied by monitoring variation of the absorbance from 230 to 730 nm. Experiments were conducted at 4 molar ratios of citrate to chloroauric acid. PCA results shows that 2 components are responsible for the variation in data. From MCR-ALS results, component 1 concentration decreases and component 2 concentration increases with time. Pure spectrum of component 1 and 2 resemble chloroauric acid and nanoparticles respectively. So, we expected that component 1 is gold salt and component 2 is nanoparticle.

Normalised pure spectra and concentration profiles obtained from MCR-ALS method at various molar ratios are shown in figures 4.10 and 4.11 respectively. The results of the analysis are the following. Irrespective of the concentration of citrate the

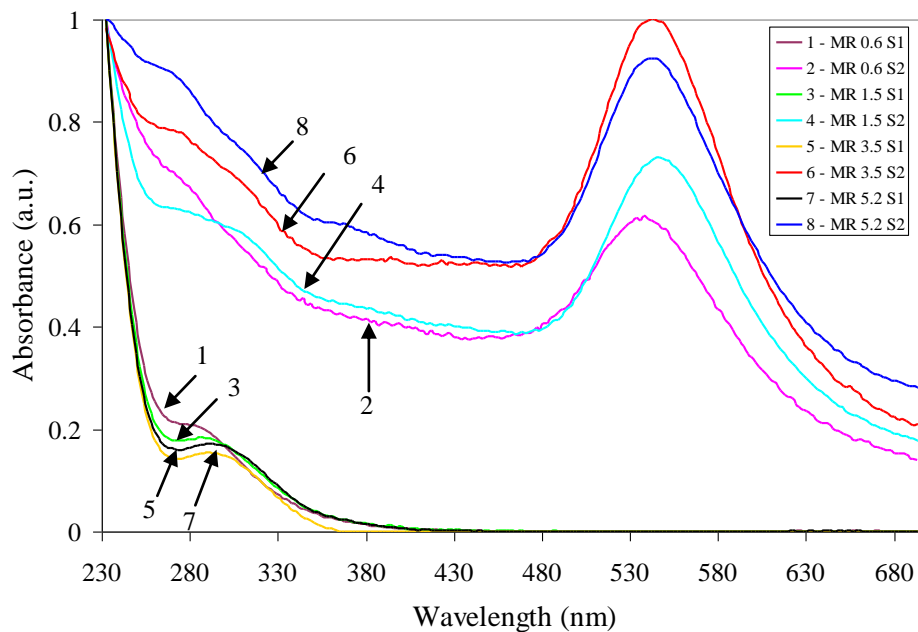


Fig. 4.10 Normalised UV-Vis spectra obtained from the MCR-ALS analysis at various molar ratios of citrate to chloroauric acid. Here S1: Chloroauric acid spectrum; S2: Nanoparticles spectrum

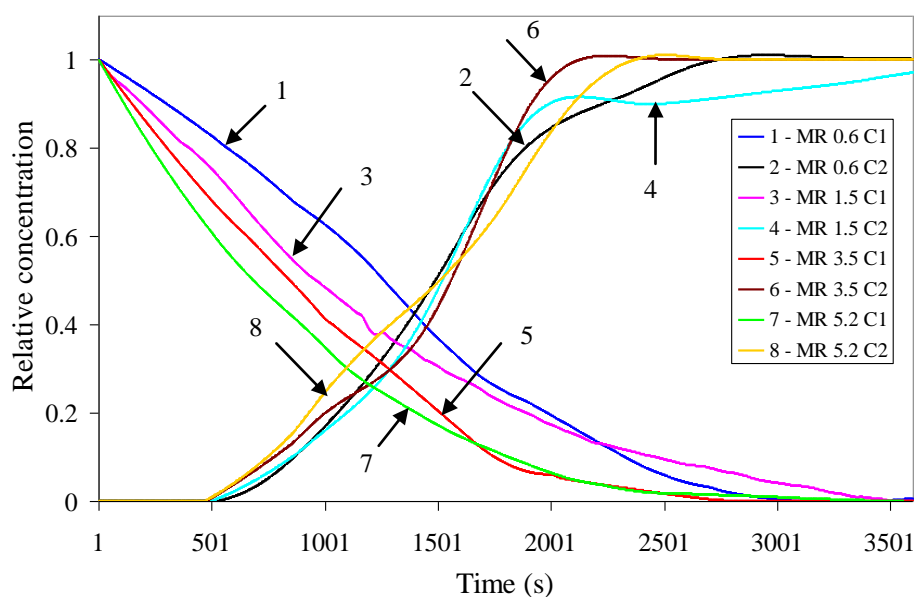


Fig 4.11 Normalised optimum concentration profiles of HAuCl_4 and nanoparticles obtained from MCR-ALS analysis. Here C1: Concentration of HAuCl_4 ; C2: Concentration of nanoparticles

absorbance peak position for nanoparticles is almost fixed. As the concentration of citrate increases rate of reduction of HAuCl_4 increases. Rate of formation of nanoparticles is independent of concentration of citrate.

Kinetics studies were carried out when 32 μM PVP stabilizer added to the reaction system. Normalised pure spectra and concentration profiles obtained from analysis are shown in figures 4.12 and 4.13 respectively. The results are similar to the results obtained without PVP. Here also absorbance peak position is independent of the citrate concentration and as citrate concentration increases rate of reduction of HAuCl_4 increases. Rate of formation of nanoparticles is independent of citrate concentration.

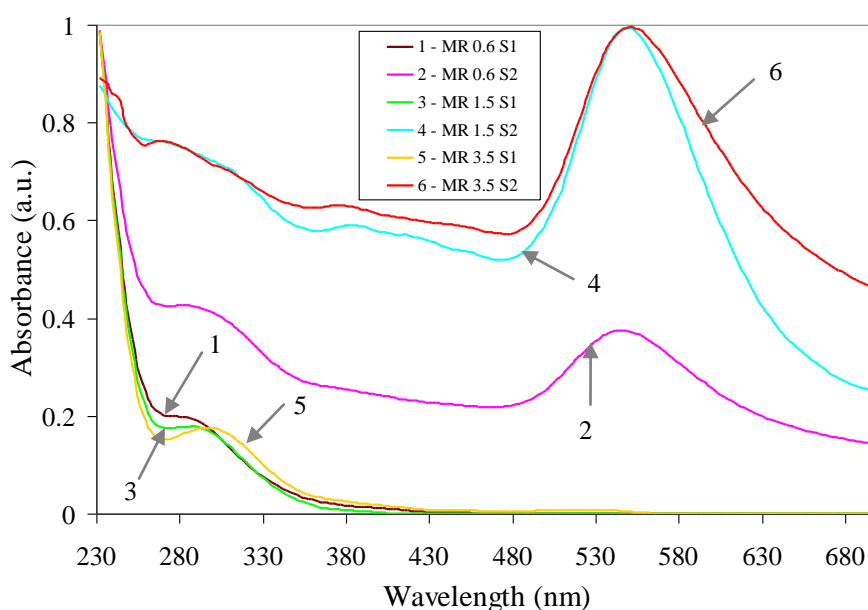


Fig. 4.12 Normalised UV-Vis pure spectra obtained from the MCR-ALS method at various molar ratios of citrate to chloroauric acid in presence of PVP. Here S1: Chloroauric acid spectrum; S2:

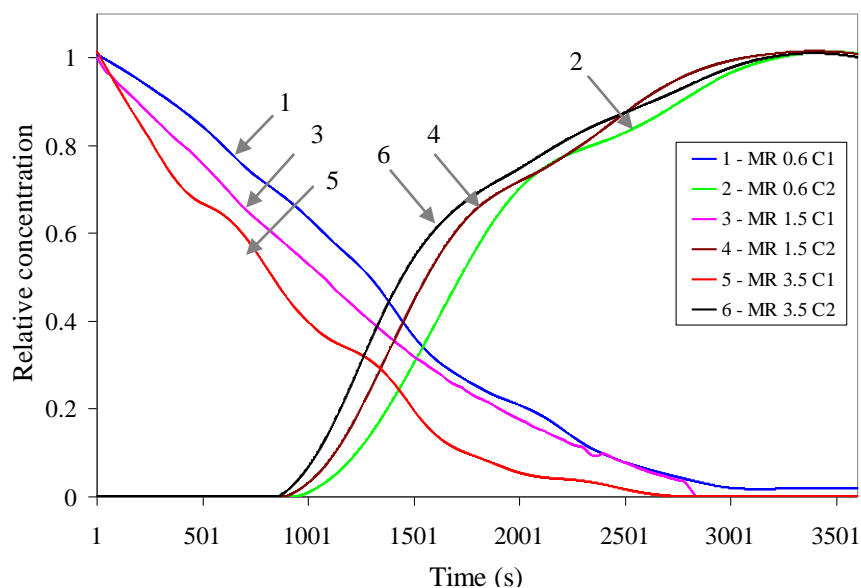


Fig 4.13 Normalised optimum concentration profiles obtained from MCR-ALS analysis at various molar ratios in presence of PVP. Here C1: Concentration of HAuCl₄; C2: Concentration of nanoparticles

Figure 4.14 compares concentration profiles for HAuCl₄ and nanoparticles obtained for with and without PVP cases. Rate of reduction of HAuCl₄ in presence and absence of PVP is almost constant. With PVP, concentration profiles for nanoparticles are raising at longer times compared to the profiles obtained for without PVP case.

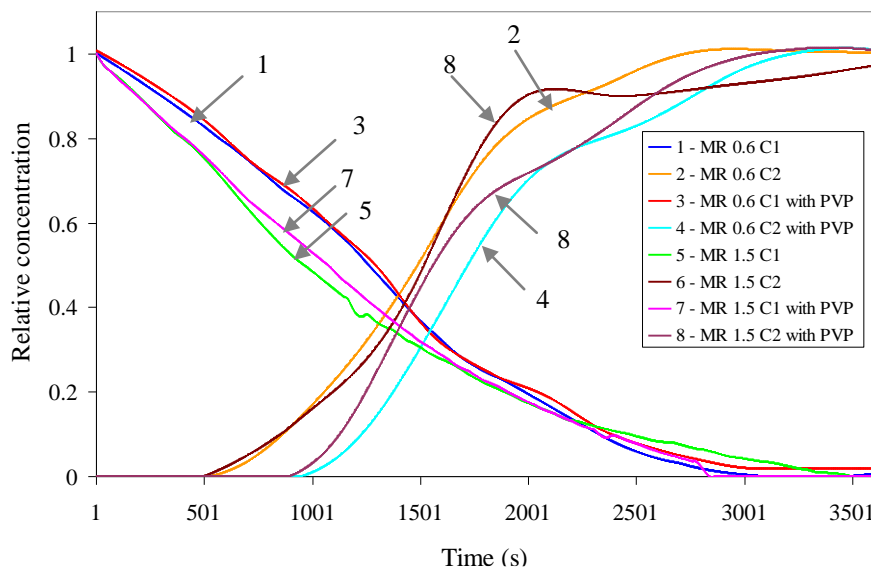


Fig 4.14 Comparison of normalised optimum concentration profiles obtained from MCR-ALS method for with and without PVP cases. Here C1: Concentration of HAuCl_4 ; C2: Concentration of nanoparticles

4.3.2 Final particle diameter

Reaction mixture volume obtained from SFM will be 70 μl . It is not possible to carry out particle measurement characterization using this volume. To find out final particle diameter for both with and without PVP cases, all experiments were conducted outside by maintaining required temperature using Peltier system. Images of the final nanoparticles solutions obtained for both without and with PVP are shown in figure 4.15.

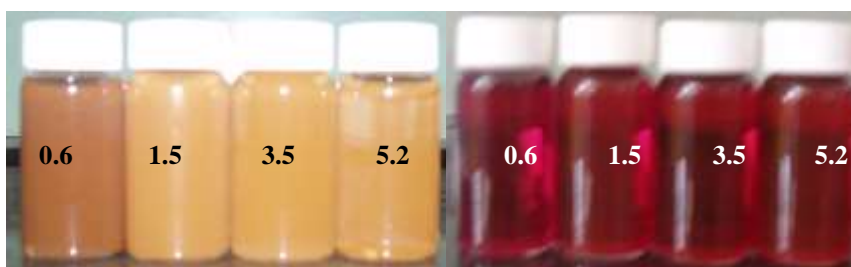


Fig 4.15 Images of the final nanoparticles solution at various molar ratios of citrate to chloroauric acid obtained for both without and with PVP cases. Colour of the solution without PVP is orange and with PVP is red.

Final nanoparticles were characterised using UV-Vis spectroscopy and scanning electron microscope (SEM). UV-Vis spectra of the final nanoparticle solution at various molar ratios for both with and without PVP are shown in figure

4.16. Without PVP absorbance peak is at more than 580 nm. Addition of PVP moves peak position to around 540 nm.

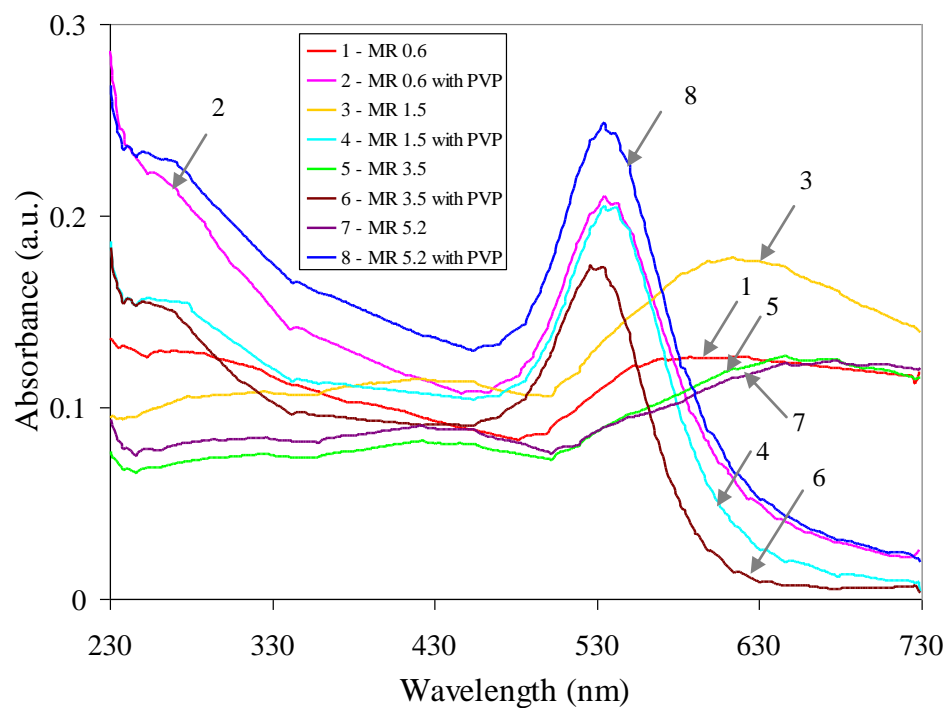


Fig. 4.16 UV-Vis spectra obtained at various molar ratios of citrate to chloroauric acid for both with and without PVP.

SEM images of the nanoparticles obtained at various molar ratios for both with and without PVP are given in appendix C. Average particle diameters are shown in table 4.1.

Molar ratio	Particle diameter without PVP (nm)	Particle diameter with PVP (nm)
0.6	210	35
1.5	290	40
3.5	155	44
5.2	145	27

Table 4.1 Average particle diameter obtained at various molar ratios of citrate to chloroauric acid for both with and without PVP.

4.4 Reason for the discrepancy in results

The final UV-Vis spectra at various molar ratios of citrate to chloroauric acid obtained from SFM was different from the UV-Vis spectra obtained from experiments conducted outside. For the lower molar ratio (MR - 0.6) in SFM, it was observed unreacted gold chloride after 1 hr. We expected that the temperature in the SFM may not be 60°C. In the literature it was reported that the UV-Vis spectrum of Reichardt's dye vary with the temperature of the solution^[6]. Variation of the peak position with temperature of the solution is shown in figure 4.17.

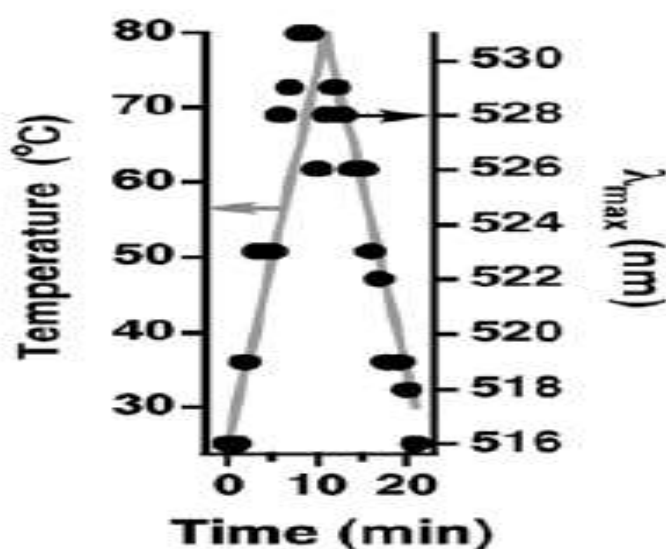
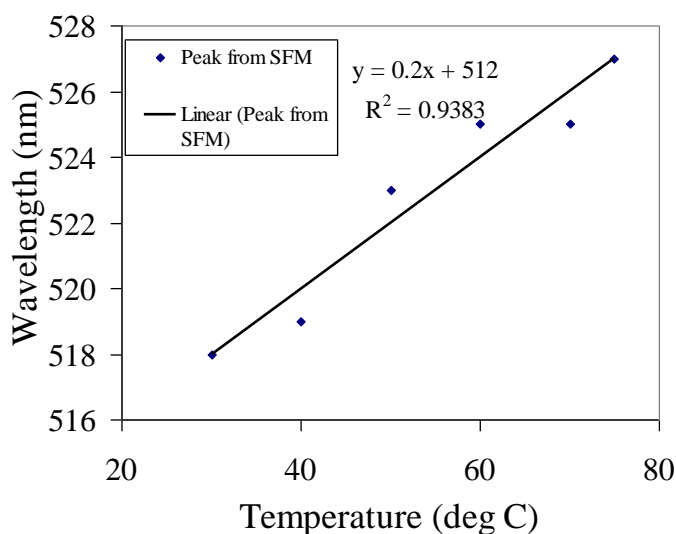


Fig 4.17 Reversible changes in absorption wavelength (λ_{max}) of a solution of Reichardt's dye in methanol as a function of temperature^[6].

We conducted dye experiments to find out exact temperature inside the UV-Vis cuvette during reaction. Variation of the peak position with temperature is shown in figure 4.18. By comparing peak position at 60⁰C with the literature values, it was concluded that the actual temperature at this temperature will be around 45-50⁰C. So in all kinetic experiments that we conducted in SFR the temperature might be less than 50⁰C.



4.5 Summary

Kinetics of gold salt reduction and nanoparticles formation at various molar ratios of citrate to chloroauric acid for with and without PVP were studied. As citrate concentration increases rate of reduction of chloroauric acid increases. Rate of formation of nanoparticles seems to be independent of concentration of citrate. Addition of PVP is not affecting reduction kinetics of gold salt; but, nanoparticles are formation observed at longer times compared to without PVP.

4.6 References

- [1]. Anusha M (2008) Investigation of gold nanoparticles formation kinetics using a stopped flow module. Master of Engineering Report, Indian Institute of Science.

- [2]. Dan V. Goia, E. Matijevic (1999) Tailoring the particle size of monodispersed colloidal gold. *Colloids and Surfaces A: Physicochemical and Engineering Aspects* 146:139–152.
- [3]. Turkevich J, Stevenson P C and Hillier J (1951) A study of the nucleation and growth processes in the synthesis of colloidal gold. *Faraday Society* 11:55-75.
- [4]. Xiaohui J, Xiangning S, Jun Li, Yubai Bai, Wensheng Y and X. Peng (2007) size control of gold nanocrystals in citrate reduction: the third role of citrate 129 : 13939-13948.
- [5]. G. Frens (1973) Controlled nucleation for the regulation of particle size in monodisperse gold suspensions. *Nature Physical Science* 241: 20-21.

Chapter 5

Modeling of formation of gold nanoparticles by tannic acid method

Synthesis of the nanoparticles in continuous flow reactors gives particles with lower polydispersity^[1]. Quantitative understanding of nanoparticle formation in flow reactors is possible only through modeling aided by knowledge of kinetics of nanoparticle formation in batch reactors. Several models have been reported in the literature regarding nanoparticle formation in batch reactors. Some of these models fitted the dynamics of nanoparticle formation by autocatalytic reaction mechanism that lacks predictive abilities over wide range of processing conditions^[2]. In this chapter, a model based on organizer mechanism^[3] is used to capture the dynamics of gold nanoparticle formation by the reduction of chloroauric acid with tannic acid.

Simple classical nucleation and growth model can't explain nanoparticle formation over a range of precursor concentrations^[3]. Kumar et al. developed an organizer based kinetic model for formation of nanoparticles by citrate method^[4]. In this kinetic model citrate reduces auric ions to auroous ions, while oxidation of citrate gives dicarboxy acetone which acts as organizer in nanoparticles formation. Chakraborty^[3] also proposed similar kind of organizer based model for nanoparticles formation by Slot method. He proposed a detailed reaction network model by considering chemistry of tannic acid along with reduction, nucleation, and growth steps. Based on experimental data on final particle size, the reaction network was further simplified. This simplified model, form the basis for modeling the data on kinetics of gold nanoparticle formation obtained by Anusha^[5].

Anusha studied the kinetics of gold nanoparticles formation by traditional way (uni-wavelength approach)^[5]. Kinetic studies were carried out at 25⁰C and 60⁰C, using various concentrations of chloroauric acid and tannic acid, while maintaining the molar ratio of tannic acid to chloroauric acid at 2.08. Variation of the absorbance at corresponding to SPR band of gold nanoparticles, with time and final particle sizes at various precursor concentrations were reported^[5]. It was found that the average particle diameter did not vary with initial precursor concentration

5.1 Mechanism of tannic acid reduction

Tannic acid is a polymer of digallic acid and glucose. Structure of tannic acid molecule is shown in figure 5.1. During reduction, the phenolic OH group present on gallic acid can be oxidized to a quinone. Due to constraint on valency of carbon, only two adjacent OH groups on each gallic acid unit are reactive. Accounting for this chemistry, and invoking the aurophilic effect of gold atoms and organizing role for moieties on tannic acid, Chakraborty J^[3] modelled tannic acid as a molecule with three independent arms in the detailed model. Reactions occur at each arm of tannic acid as shown in figure 5.2.

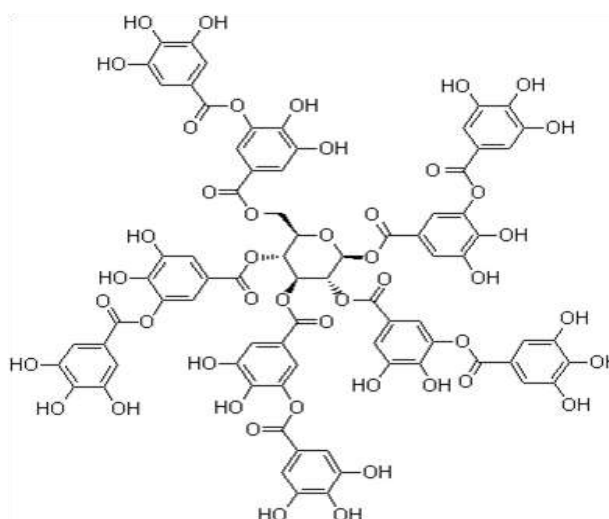


Fig. 5.1 Schematic of tannic acid molecular structure^[3].

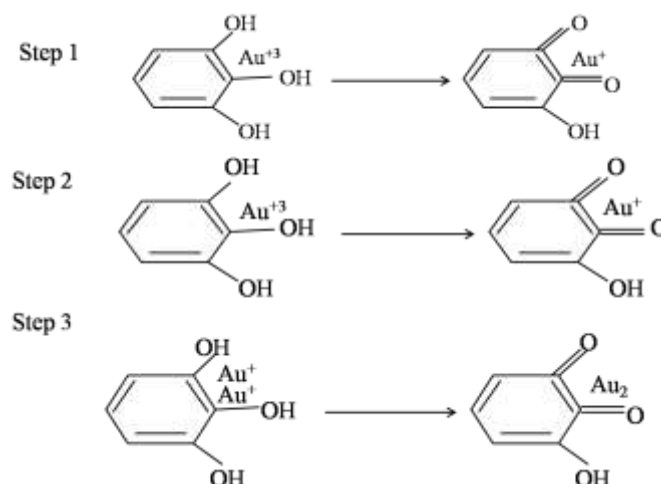


Fig. 5.2 Steps involved at each arm of tannic acid. Step 1 and 2: Reduction of two auric ions to aurous ions by gallic acid molecules. Step 3: Reduction of dimer of aurous ion to dimer of gold atoms by gallic acid molecule, the formed gold dimer is weakly bonded to the reduced form of gallic acid^[3].

Chakraborty^[3] considered tannic acid as a molecule of two arms in simplified model. Various forms of tannic acid species during nanoparticles formation are shown in figure 5.3.

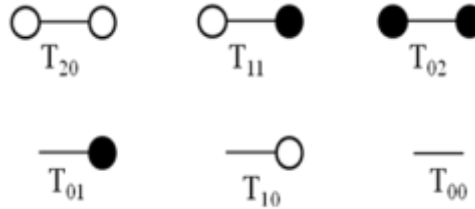


Fig. 5.3 Various forms of tannic acid species present during nanoparticle formation; In T_{ij} notation i represents unreacted arms and j represents loaded arms^[3]

5.2 Nucleation and growth mechanisms

It was proposed that only tannic acid with two arms loaded can undergo nucleation and form nucleus as shown in figure 5.4 (a). Therefore, expression for the rate of nucleation is^[3]

$$\frac{dN}{dt} = k_n T_{02} \quad (5.1)$$

where N is number of particles per unit physical volume. k_n is nucleation rate constant. T_{02} is concentration of tannic acid with two arms loaded.

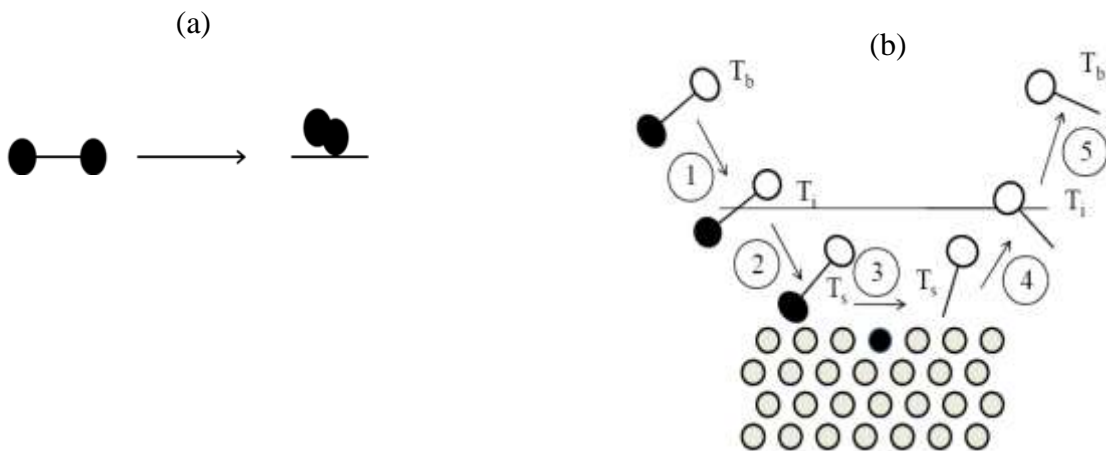


Fig. 5.4 Mechanism of nucleation and growth in nanoparticles formation. (a). Formation of nucleus by tannic acid with two arms loaded. (b). Steps involved in growth process 1). Mass transfer of loaded tannic acid to the surface. 2). Adsorption of tannic acid. 3). Surface reaction. 4). Desorption of reacted tannic acid. 5). Mass transfer of reacted tannic acid to bulk phase^[3].

It was also proposed that only tannic acid with at least one arm loaded can participate in growth process. The various steps involved in growth process [namely diffusion, dissolution, incorporation and desorption] are shown in figure 5.4 (b). If surface reaction and desorption steps are controlling steps, then, expression for the growth process is^[3]

$$G_{ij} = \frac{k_g T_{ij}^*}{k_d + T_{ij}^*} \quad (5.2)$$

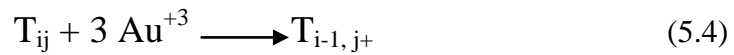
where k_g is growth constant, k_d is desorption constant and T_{ij}^* is tannic acid concentration at the surface of the particle. Expression for the T_{ij}^* can be obtained by balancing flux due to diffusion and rate of growth^[2].

$$k_L (T_{ij} - T_{ij}^*) = \frac{k_g T_{ij}^*}{k_d + T_{ij}^*} \quad (5.3)$$

where k_L is mass transfer coefficient and T_{ij} is concentration of tannic acid in bulk phase.

5.3 Model equations

For simplified model, overall reaction network by considering all possible interactions is shown in figure 5.5. General expression for reduction of trivalent gold to gold atoms is



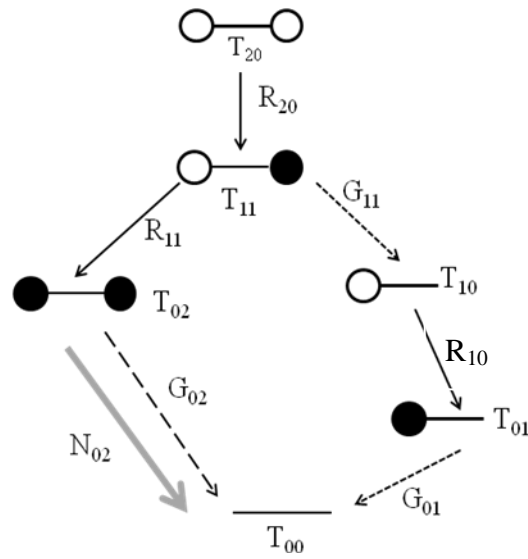


Fig. 5.5 Reaction net work by considering all possible interactions in formation of nanoparticles using chloroauric acid and tannic acid as precursors^[3].

In model, individual order of reaction with respect to tannic acid and gold salt were taken as 1 and 1.5 respectively. General expression for the rate of reaction is

$$R_{ij} = k_r [T_{ij}]^1 [M]^{1.5} \quad (5.5)$$

where k_r is rate constant, $[]$ is concentration, T_{ij} represents tannic acid forms, M represents chloroauric acid. The rate of change of concentration of various species can be written as^[3]

$$\frac{dT_{20}}{dt} = -k_r [T_{20}]^1 [M]^{1.5} \quad (5.6)$$

$$\frac{dT_{11}}{dt} = k_r [T_{20}]^1 [M]^{1.5} - k_r [T_{11}]^1 [M]^{1.5} - G_{11} A \quad (5.7)$$

$$\frac{dT_{02}}{dt} = k_r [T_{11}]^1 [M]^{1.5} - k_n [T_{02}] - G_{02} A \quad (5.8)$$

$$\frac{dT_{10}}{dt} = -k_r [T_{10}]^1 [M]^{1.5} + G_{11} A \quad (5.9)$$

$$\frac{dT_{01}}{dt} = k_r [T_{10}]^1 [M]^{1.5} - G_{01} A \quad (5.10)$$

$$\frac{dT_{00}}{dt} = G_{02} A + G_{01} A + k_n [T_{02}] \quad (5.11)$$

$$\frac{dM}{dt} = -3k_r M^{1.5} \left[[T_{20}]^1 + [T_{11}]^1 + [T_{01}]^1 \right] \quad (5.12)$$

where G_{ij} is growth rate and A is total surface area per unit physical volume of all particles. The rate of change of individual particle concentration is

$$\frac{dN_2}{dt} = k_n T_{02} - G A_2 N_2 \quad (5.13)$$

$$\frac{dN_i}{dt} = -G A_i N_i + G A_{i-1} N_{i-1} \quad \text{for } i = 3 \text{ to } i_{\max} \quad (5.14)$$

where $G = \sum_{i=0}^1 \sum_{j=1}^2 G_{ij}$

Equation (5.14) is a generalized discrete population balance equation (PBE) for pure growth process. The number of discrete PBEs to be solved depends on the size of the final particle and they are very large for larger particles. The problem of solving large number of discrete PBEs can be reduced by introducing moments of the population^[6] into the model to simplify model equations. Generalized expression for the j^{th} moment assuming infinite population is

$$\frac{d \sum_{i=3}^{\alpha} i^j N_i}{dt} = - \sum_{i=3}^{\alpha} i^j G A_i N_i + \sum_{i=3}^{\alpha} i^j G A_{i-1} N_{i-1} \quad (5.15)$$

For $j=1/3, 2/3$ and 1 this equation gives expressions for rate of change of perimeter, surface area and volume of particles by simplifying and multiplying with appropriate pre-factors.

$$\frac{d \sum_{i=2}^{\alpha} P_i N_i}{dt} = P_a A_v^2 A_a G (N - N_2) + P_2 N_2 A_v + A_2 P_3 A_v^2 N_2 G \quad (5.16)$$

$$\frac{d \sum_{i=2}^{\alpha} A_i N_i}{dt} = 2A_a^2 \left(\frac{A_v}{P_a} \right) G \sum_{i=3}^{\alpha} P_i N_i + A_2 N_2 A_v + A_2 A_3 A_v^2 N_2 G \quad (5.17)$$

$$\frac{d \sum_{i=2}^{\alpha} V_i N_i}{dt} = 3V_a A_v G \sum_{i=3}^{\alpha} A_i N_i + V_2 N_2 A_v + V_3 A_v^2 A_2 N_2 G \quad (5.18)$$

The volume of nanoparticles is correlated with experimentally determined absorbance value at SPR maximum based on application of Mie's theory (refer appendix B). In model absorbance is calculated using the following expression

$$A = kV \quad (5.19)$$

The proportionality constant k is obtained by plotting absorbance and total particle volume at various concentrations. If we assume infinite population size, then, the rate of change of total number of particles is

$$\frac{dN}{dt} = k_n T_{02} \quad (5.20)$$

Volume average diameter (D_v), surface area average diameter (D_s) and perimeter average diameter (D_p) are calculated using the following expressions^[6]

$$D_v = \left[\left(\frac{6}{\pi} \right) \left(\frac{V}{N A_v} \right) \right]^{1/3} \quad (5.21)$$

$$D_s = \left[\left(\frac{1}{\pi} \right) \left(\frac{A}{N A_v} \right) \right]^{1/2} \quad (5.22)$$

$$D_p = \left[\left(\frac{1}{\pi} \right) \left(\frac{P}{N A_v} \right) \right] \quad (5.23)$$

COV is defined as the ratio of standard deviation in particle distribution to the average particle diameter.

$$COV = \frac{\sigma}{D_v} \quad (5.24)$$

Expression for the standard deviation is

$$\sigma = \left[D_s^2 - D_p^2 \right]^{1/2} \quad (5.25)$$

Model equations are solved in MATLAB environment (version 7.3) using ode 15S solver (refer appendix D) with appropriate initial conditions.

5.4 Model results for 25⁰C

The best parameter values given in table 5.1 were obtained by fitting model predictions to experimental data at one concentration using Berkeley Madonna [refer appendix D]. The same parameter values were used to get model predictions at other concentrations. Figure 5.6 shows evolution of the absorbance obtained from experiment and predicted from model. On linear plot, model predictions are following experimental curves very well. But, on semilogarithmic plot a kink is seen at early stages. The reason for kink may be following. Once nuclei forms, they will grow by autocatalytic growth process due to the presence of large pool of loaded tannic acid molecules. Concentration of the loaded tannic acid molecules (both T_{11} and T_{02}) falls suddenly due to the huge surface area available for growth process. When concentration of loaded tannic acid molecules fall to certain value, chemical reaction which is responsible for formation of loaded tannic acid molecules controls the growth process. At the kink transition from auto catalytic growth to chemical reaction controlled growth takes place.

Parameter	value	Units
k_r	0.101	$(\text{mol}/\text{m}^3)^{-1.5} \text{s}^{-1}$
k_g	3.53×10^{-4}	$\text{mol}/\text{m}^2 \text{s}$
k_d	0.0104	mol/m^3
k_n	5	s^{-1}
k	2	m/s

Table 5.1 Best fit parameter values for predicting experimental results for formation gold nanoparticles by tannic acid method at 25⁰C

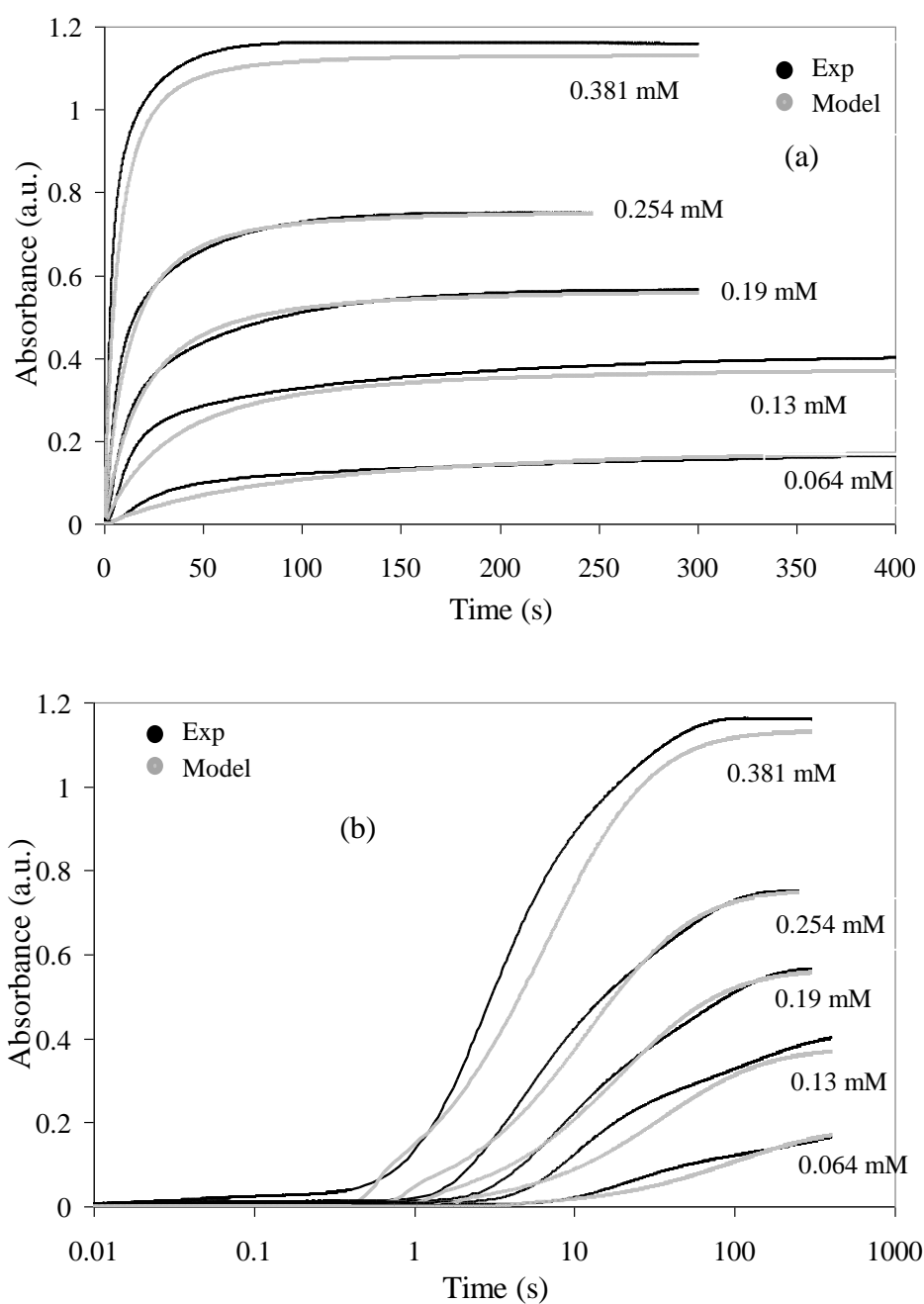


Fig. 5.6 Time evolution of absorbance obtained from experiment and predicted from model at various initial concentrations of gold chloride at 25°C. (a). Evolution on linear plot. (b). Evolution on semilogarithmic scale.

Table 5.2 compares particle diameter obtained from experiment and predicted from model at various concentrations. Experimental determined diameter was the hydrodynamic diameter; the actual diameter of the metal core is expected to be 3 nm less than the hydrodynamic diameter^[7]. The core diameter is found to be independent of initial concentration and the variation is within experimental error. The size variation predicted by model is also well within experimental error indicating that model predictions of mean nanoparticle size are accurate. Model is predicting that COV is also almost constant for the concentration range that the data available. Unfortunately, experimental COV was not reported.

Conc. of H _{Au} Cl ₄ (mM)	Experimental DLS diameter (nm) \pm standard deviation	Expected core Diameter (nm)	Model diameter (nm)	Model COV (%)
0.381	-	-	7.1	20
0.254	10.1 \pm 1.8	7.1	7.3	20
0.19	11.3 \pm 1.2	8.3	7.5	21
0.127	11.6 \pm 1.5	8.6	7.6	21
0.064	11.2 \pm 1.0	8.2	7.6	18

Table 5.2 Comparison of the particle diameter obtained from experiment and predicted from model for the formation of gold nanoparticles by tannic acid method at 25°C

Figure 5.7 shows variation of concentrations of different forms of tannic acid species with time. At the start of reaction only T₁₁ and T₀₂ are formed. T₀₂ plays the same role as monomer species in supersaturated solution of classical nucleation (refer chapter 2). As reaction progresses concentration of T₀₂ increases and it is responsible for the formation of nucleus. The nucleation process continues until enough surface area is created while the formed nuclei participate in growth process. The concentration of T₀₂ falls precipitously because of simultaneous nucleation and autocatalytic growth processes. The concentration of T₀₁ increases until nucleation process starts and after that it decreases due to consumption of it in growth process.

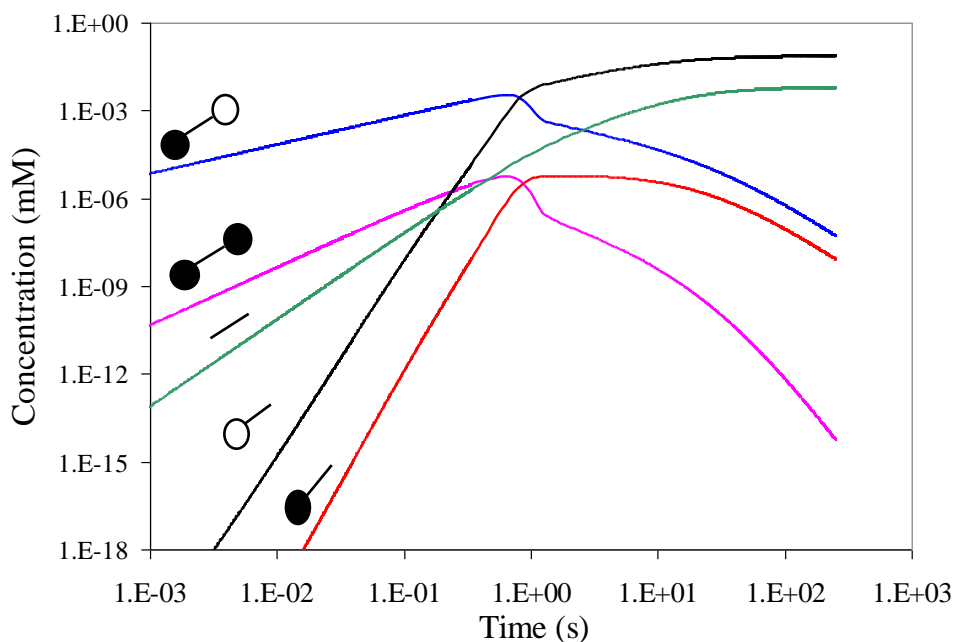


Fig. 5.7 Concentration profiles of various forms of tannic acid during formation of gold nanoparticles at 25°C by tannic acid method for case of 0.254 mM HAuCl_4 initial concentration

Variation of the concentration of chloroauric acid and rate of nucleation with time are shown in the figure 6.8 for 0.254 mM concentration. Around 10 % of the chloroauric acid is reduced by the time nucleation gets completed.

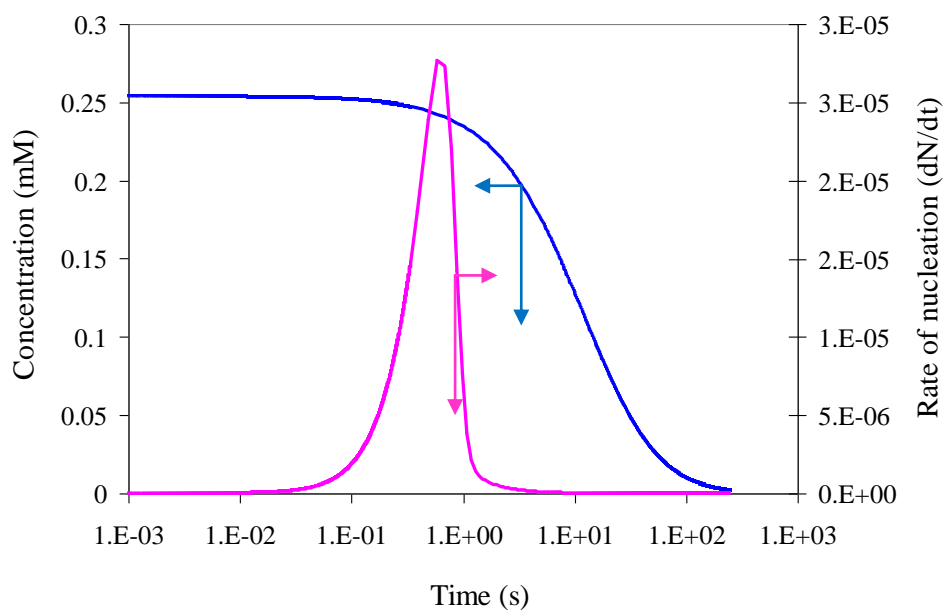


Fig. 5.8 Variation of the concentration of chloroauric acid and rate of nucleation with time for case of 0.254 mM HAuCl_4 initial concentration at 25°C in formation of gold nanoparticles by tannic acid method initial concentration.

5.5 Model results for 60°C

The model is predicting experimental data by just increasing rate of reaction by 3 times and keeping all other parameters are same as that of 25°C. The parameter values for 60°C are given in table 4.3. Evolutions of the absorbance profiles obtained from experiment and predicted from model are shown in figure 4.9. The trends are very similar to that seen at 25°C. Particle diameter obtained from experiment and model at all concentrations are given in table 4.4. Variation of the concentrations of tannic acid species with time are shown in figure 4.10 for 0.254 mM concentration. Rate of change of concentration of chloroauric acid and rate of nucleation with time are shown in figure 4.11. Around 70 % of the chloroauric acid has reacted by the time taken for nucleation process to stop.

Parameter	value	units
k_r	0.101	$(\text{mol/m}^3)^{-1.5} \text{s}^{-1}$
k_g	3.53×10^{-4}	$\text{mol/m}^2 \text{s}$
k_d	0.0104	mol/m^3
k_n	5	m/s
k_l	2	s^{-1}

Table 5.3 Best fit parameters to predict experimental results for the formation of nanoparticles by tannic acid method at 60°C

Conc. of HAuCl ₄ (mM)	Experimental diameter (nm)± Standard deviation	Expected core diameter (nm)	Model diameter (nm)	Model COV (%)
0.381	-	-	5.7	20
0.254	8.7 ± 1.5	5.7	5.9	21
0.19	8.1 ± 2.3	5.1	6.0	21
0.127	9.1 ± 1	6.1	6.2	21
0.064	12.0 ± 4.2	9.0	6.5	19

Table 5.4 Comparison of the experimental results with model predictions for the formation of nanoparticles by tannic acid method at 60°C

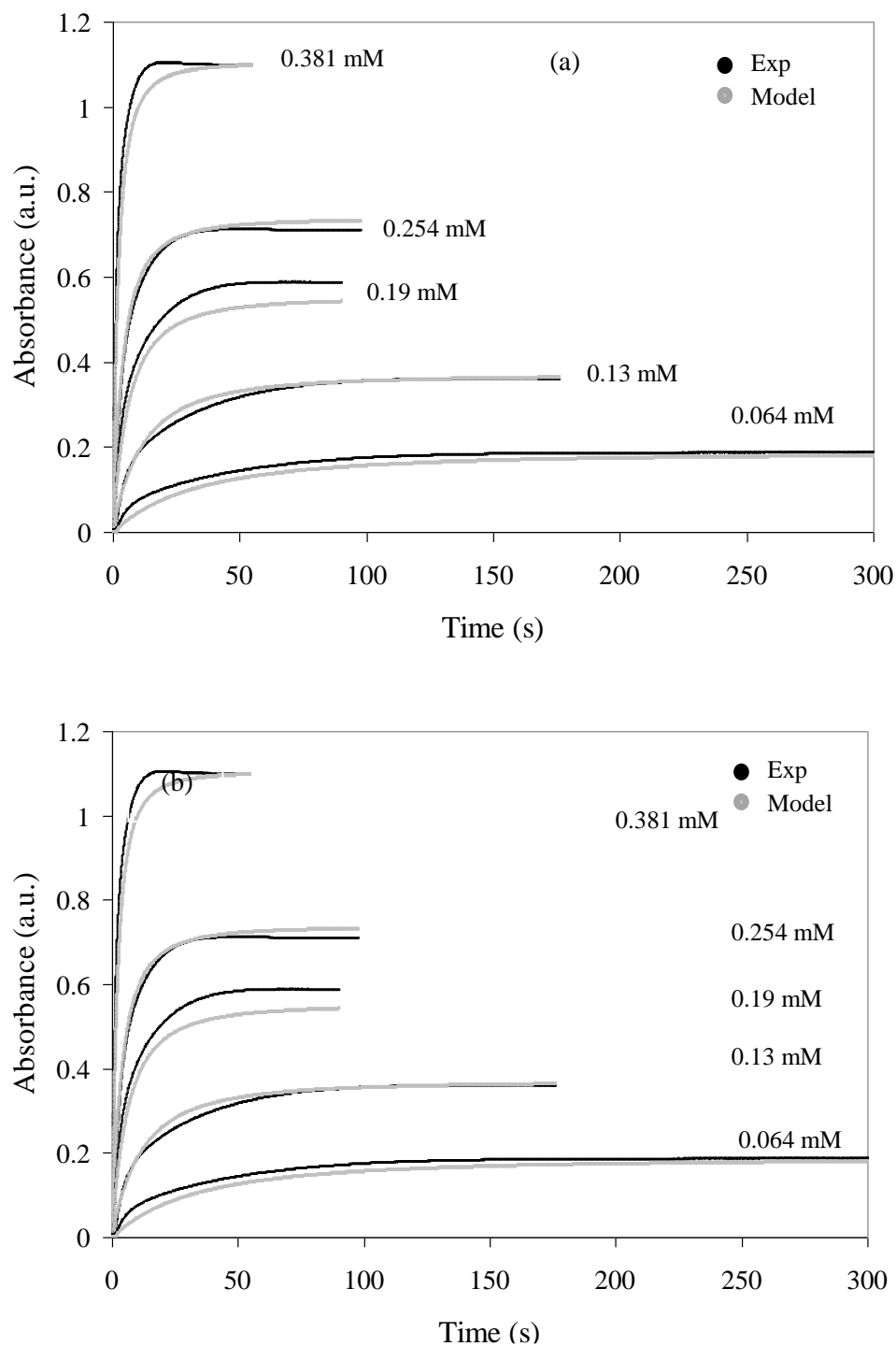


Fig. 5.9 Time evolution of the absorbance obtained from experiment and model at various initial concentrations of gold chloride at 60°C. (a). Evolution on linear plot. (b). Evolution on semilogarithmic plot.

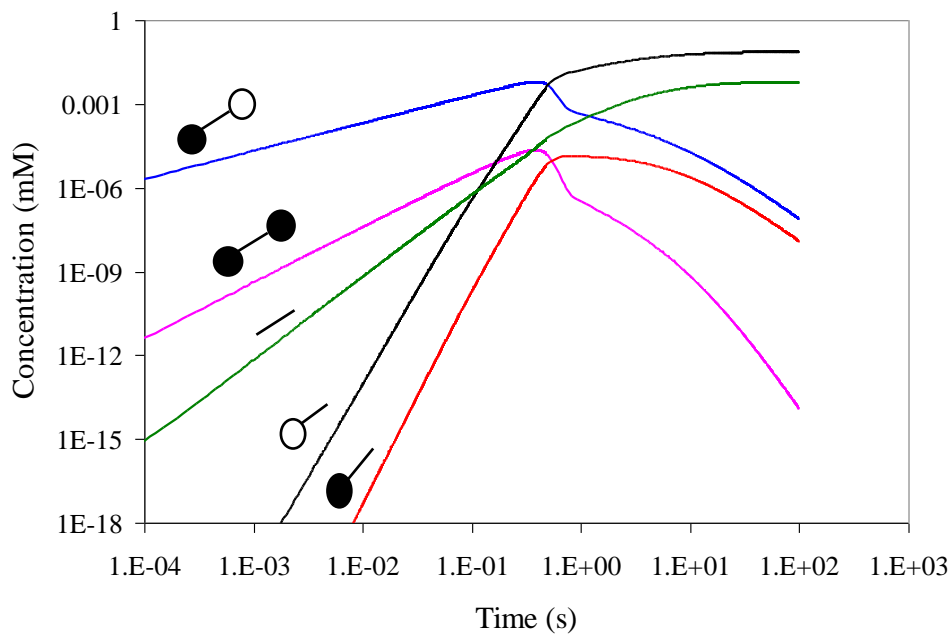


Fig. 5.10 Concentration profiles of various forms of tannic acid during formation of gold nanoparticles at 25°C for the case of 0.381 mM HAuCl_4 of initial concentration by tannic acid method

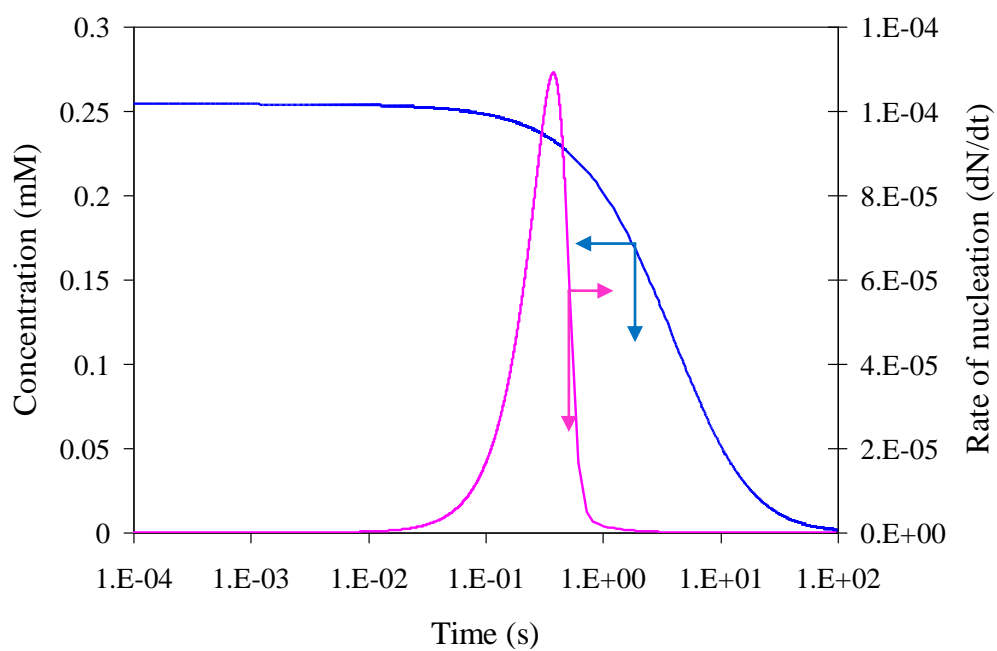


Fig. 5.11 Variation of the concentration of number of particles per unit volume and chloroauric acid with time at 60°C in the formation of gold nanoparticles for the case of 0.381 mM HAuCl_4 by tannic acid method.

5.6 Parameter Sensitivity

Parameter sensitivity was carried out to find out effect of various parameters on evolution curve and final particle size. All parameters other than k_1 effect final particle diameter. Growth process is controlled by either only surface reaction or chemical reaction, because of this fact k_1 , which is characteristic of diffusion process, is affecting neither evolution curve nor particle diameter. Effect of various parameters on absorption evolution curve is shown in figure 5.12. Out of all parameters, evolution curve is very sensitive to the k_r . Table 5.5 shows effect of parameters on final particle size. Parameter k_g is affecting particle diameter much compared to others.

Parameter	Parameter*1.2	Particle diameter (nm)
k_r	0.121	7.6
k_g	4.8×10^{-4}	8.1
k_d	0.0108	7.3
k_n	6	7.5

Table 5.5 Effect of various parameters on final particle size. Compared other parameters k_r effects more.

5.7 Summary

Simplified organizer based model of Chakraborty is found to explain most of the experimental observed dynamics of gold nanoparticle formation by reduction of HAuCl_4 by tannic acid. The ability to predict dynamics over a wide concentration and temperature range fosters confidence in the utility of this reaction network model. This will be further validated, by incorporating it into appropriate models of flow reactors, utilizing experimental data from microfluidic reactors in future. The information obtained from kinetics and modeling of nanoparticle formation in batch reactors can be used for modeling of the nanoparticles formation in microfluidic devices.

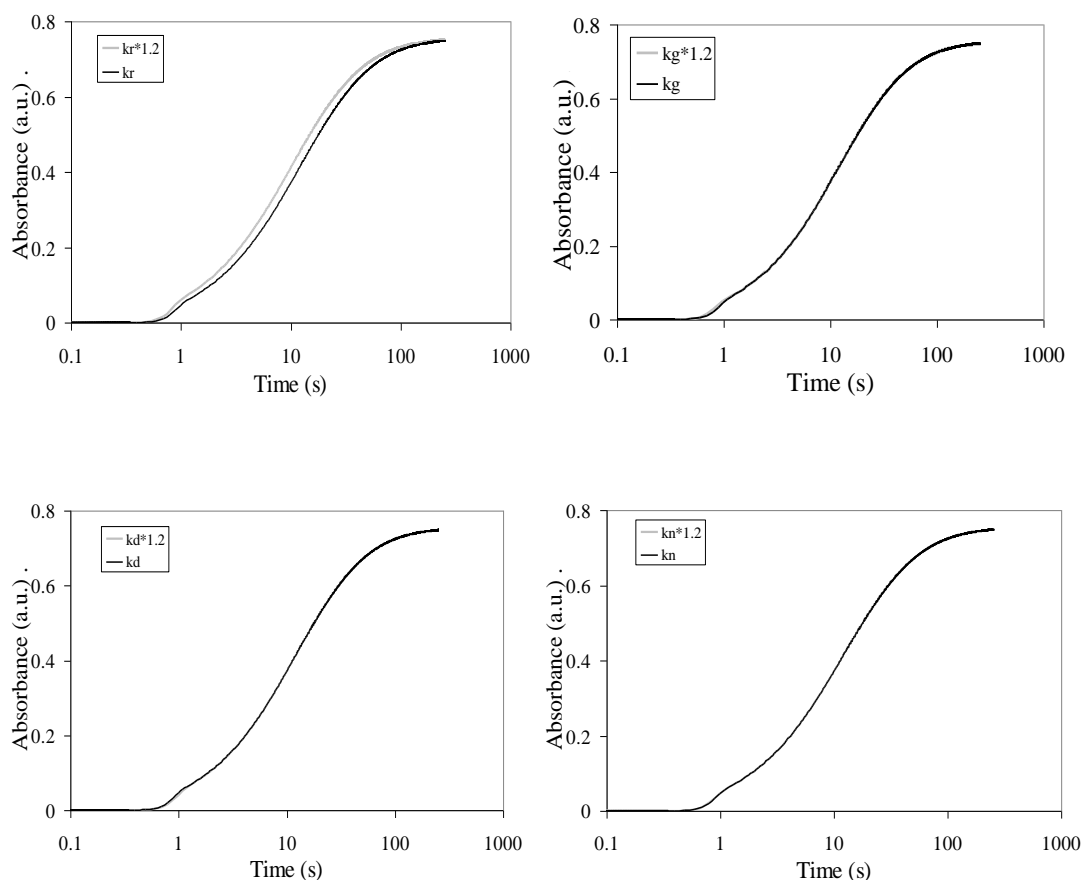


Fig. 5.12 Effect of various parameters on evolution curve. Out of all parameters parameter k_r effects evolution curve more.

5.8 References

- [1]. David S, Robert C.R. Wootton, Richard F. Winkle, Ben F. Cottam, Ramon Vilar, Andrew J. deMello, C. Paul Wilde (2007) Synthesis of thiol functionalized gold nanoparticles using a continuous flow microfluidic reactor. *Materials Letters* 61: 1146–1150.
- [2]. Finney E E, Finke G R (2007) Nanocluster nucleation and growth kinetic and mechanistic studies: A review emphasizing transition metal nanoclusters. *Journal of Colloidal and Interface Science* 317: 351-374.
- [3]. Chakraborty J (2008) Modeling and Simulation Frameworks for Synthesis of Nanoparticles. PhD Thesis, Indian Institute of Science.

- [4]. Kumar S, Gandhi K S, Kumar R (2007) Modeling of formation of gold nanoparticles by citrate method. *Industrial Engineering Chemistry and Research* 46:3128-3136
- [5]. Anusha M (2008) Investigation of gold nanoparticles formation kinetics using a stopped flow module. Master of Engineering Report, Indian Institute of Science.
- [6]. Sivaramakrishna P (2006) Modeling of synthesis of thiol-coated gold nanoparticles. Master of Engineering Report, Indian Institute of Science.
- [7]. Through personal communication with Sankar Kalidas (PhD scholar, Dept. of Chemical Engg., IISc), it was informed that core diameter of a particle is always 3 nm lesser than the DLS diameter for tannic acid protocol.

Chapter 6

Summary and Recommendations

MCR-ALS method was implemented for analysis of 3D UV-Vis spectroscopic data of nanoparticle formation. The analysis method was validated by analysing known generated evolving spectroscopic data. The UV-Vis spectroscopic data obtained during gold nanoparticles formation by citrate method was analysed using analysis method. The analysis results were in concord with the experimental observations.

UV-Vis spectrum of chloroauric acid, tannic acid and sodium citrate was sensitive to the solution pH. Chloroauric acid was decomposing in presence of UV light. When chloroauric acid solution is exposed to UV-Vis light around 24 % of the chloroauric acid is getting decomposed with in 150 s. By controlling light source shutter using Keithley AC and DC light source we were able to reduce decomposition to 3 %.

Analysis results obtained by analysing the UV-Vis spectroscopic data at various ratios of citrate to chloroauric acid for both with and without PVP gives the following deductions

1. As the concentration of citrate increases rate of reduction chloroauric acid increases. Rate of formation of nanoparticles is independent of citrate concentration. The particle diameter also seems to be independent of citrate concentration.
2. Addition PVP is not affecting kinetics of chloroauric acid reduction. But, in presence of PVP nanoparticle formation was observed at longer times compared to without PVP.
3. Addition of PVP gives smaller particles compared to without PVP.

Simplified model of Chakraborty predicts the kinetics of gold nanoparticles formation by tannic acid method over a wide concentration and temperature range. Model results are giving some extra insight about rate of reduction of chloroauric acid and rate of nucleation. The information obtained in batch reactors can be used for modeling of nanoparticle formation in flow reactors.

Recommendations

- For better understanding of the kinetics of gold nanoparticles formation in citrate method, all experiments should be conducted with 10 mm path UV-Vis quartz cuvette.
- Modelling studies on kinetics of nanoparticle formation for both without and with PVP has to be carried out to understand effect of PVP on kinetics completely.

Appendix – A

Instrumentation and Performance of Mixing

A.1 Experimental set up

Stopped flow module from Biologic SAS (SFM-400) enables the study of kinetics of the rapid reactions by allowing rapid mixing (time scale of ms) of the reagent precursors. It uses motor driven syringes coupled with modern microprocessor techniques for the accurate control on the flow rates. A high power UV-Vis fiber light source from Hamamatsu is used for optical system. A J&M diode array detector is used for rapid data acquisition in the range 0.8 – 32 ms over all wavelengths from 190 – 730 nm. Dead time depends on the type of the cuvette and for the TC-100/10F, it is 3 ms at a flow rate of 10 ml/s ^[1]. Schematic of experimental set up is shown in figure A.1 (a).

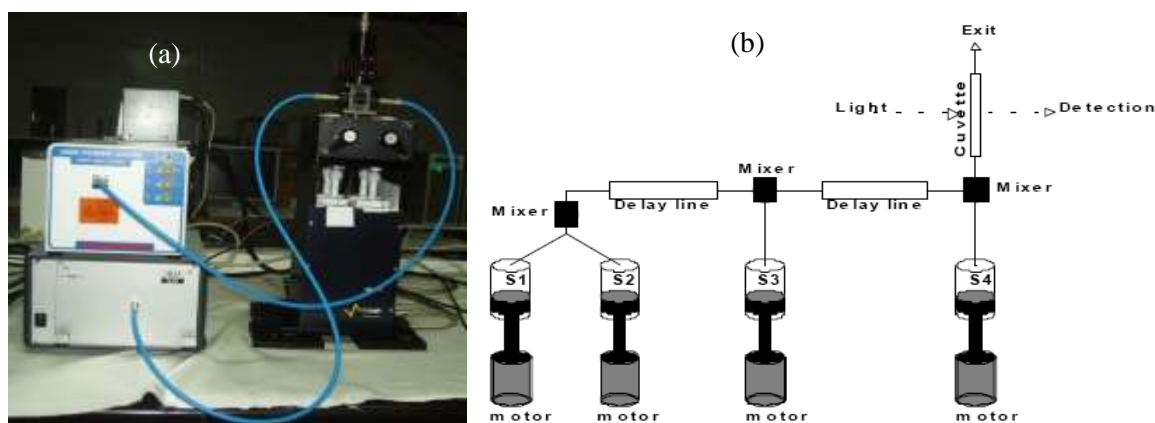


Fig. A.1 (a) Image of experimental set up. (b) Stopped flow module with four syringes and two delay lines, operating in stopped flow mode^[1]

Stopped flow module has a provision either to operate in stopped flow mode or quenched flow mode. Schematic representation of the SFM-400 operating in stopped flow mode is shown in the figure A.1 (b). The reagents coming from syringes S₁ and S₂ get mixed first, then reagents from the syringe S₃ get mixed after a variable delay line and finally it is mixed with the contents of the syringe S₄ after passing through another variable delay line ^[1].

Stopped flow module uses Berger ball mixers for the rapid mixing of the reactant precursors. In Berger ball mixers, turbulent wake created behind a hemisphere is responsible for mixing. Schematic diagram for the mixing of the solutions in Berger ball mixer is shown in figure A.2. Solutions A & B meet at a point 1 where break up of the jets and initial mixing takes place. The partially mixed solutions travel around a hemisphere and reaches point 2. Before reaching point 2 the solutions pass through a region of intense turbulence where rapid mixing takes place [2].

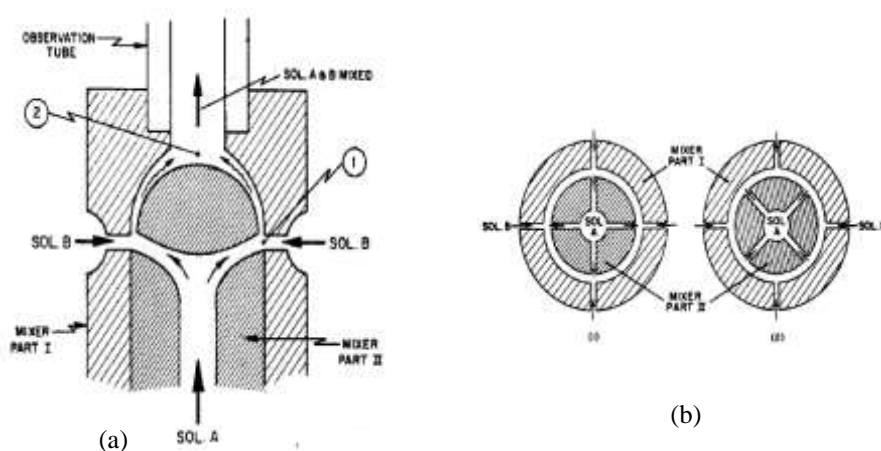


Fig. A.2 (a) Schematic of Berger ball mixer showing mixing of the solutions. (b) Orientation of jets. (1). Jets coming at 0° ; Jets coming at 45° [2].

A.2 Performance of mixing

Preliminary tests were carried out to check performance of mixing in SFM. 1 μM Dichloroindophenol (DCIP) stock solution was prepared. Syringes S1, S2 and syringes S3, S4 were filled with DCIP and DI water respectively. Various mixing ratios from syringes were maintained to get desired volumetric ratios of DCIP and DI water. UV-Vis spectrum was recorded at each mixing ratio. DCIP and DI water were mixed manually outside at various volumetric mixing ratios and UV-Vis spectrum was recorded using Systronics UV-Vis spectrophotometer. Figure A.3 shows UV-Vis spectrum at various mixing ratios obtained from SFM and systronics spectrophotometer. This indicates that the mixing within SFM is complete for the volumetric ratios studied. Figure A.4 shows variation of the absorbance at 608 nm with concentration of DCIP. Absorbance is varying linearly up to 0.9.

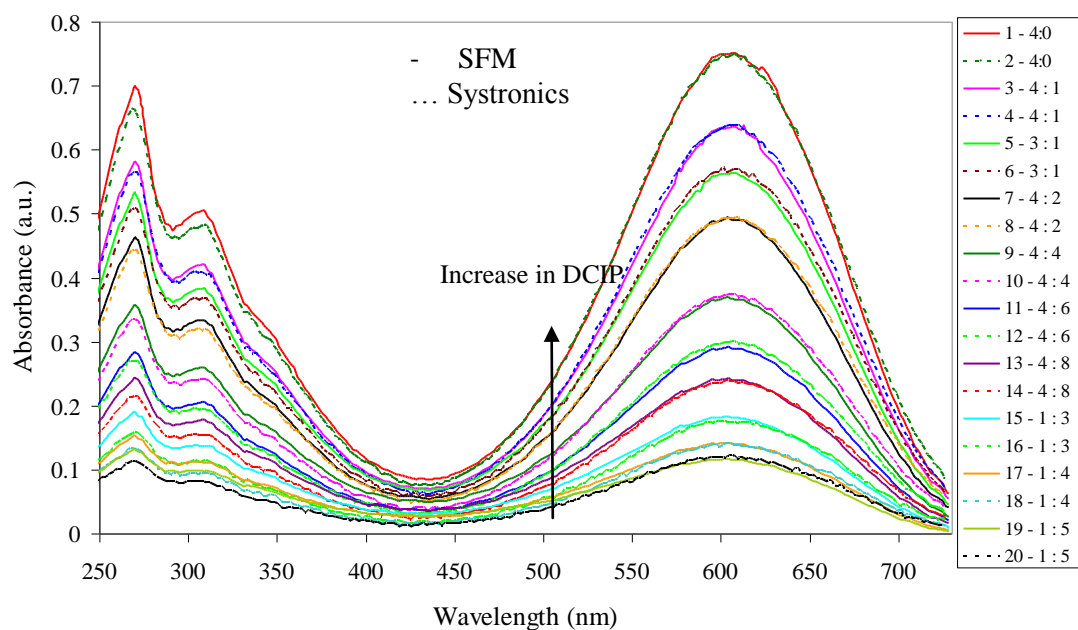


Fig. A.3 UV-Vis absorption spectrums for the solutions with various volume ratios of DCIP and DI water obtained from SFM and Systronics spectrophotometer. Solid line: SFM; Dotted line : Systronics

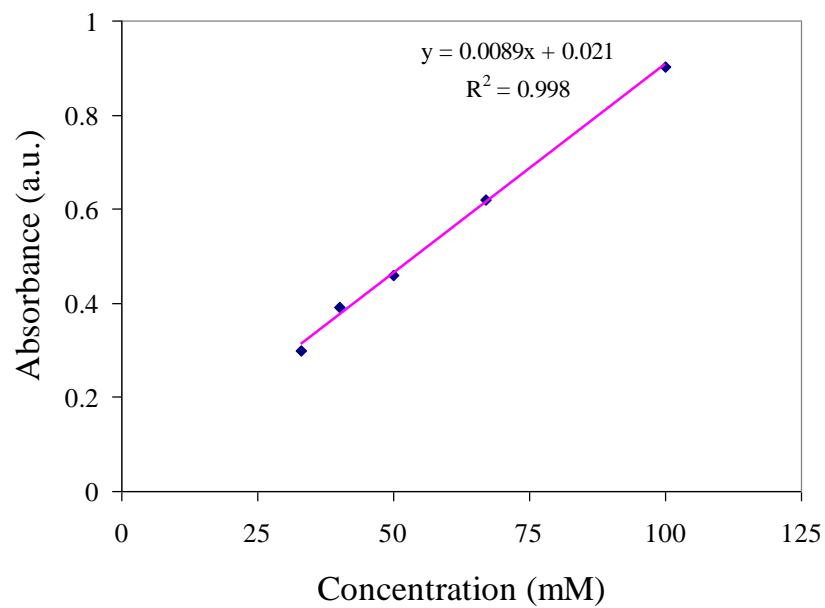


Fig A.4 Variation of the absorbance with concentration of DCIP. Absorbance is varying linearly up to 0.9.

A.3 References

- [1]. <http://www.bio-logic.info/rapid-kinetics/> accessed on 22/07/08
- [2]. Berger R L, Balko B, Chapman H F (1967) High resolution mixer for the study of the kinetics of rapid reactions in solution. *The Review of the Scientific Instruments* 39 (4):493-498

Appendix - B

Surface plasmon resonance (SPR)

SPR is the coherent excitation of all the free electrons within the conduction band. When nanoparticle is placed in an electric field, displacement of the conduction band electrons with respect to the centre of the mass of ions in the solid takes place as shown in the figure B.1. This gives rise to a net charge difference at the nanoparticle surface which results in a restoring force. This process causes dipolar oscillation of the electrons and when the frequency of the incident electric field matches the resonant frequency of the dipolar oscillation, it results in enhanced absorption called SPR.

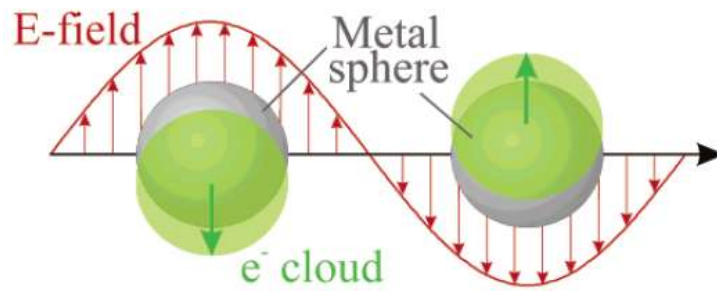


Fig. B.1 Schematic of the surface plasmon resonance for sphere, showing the displacement of the conduction band electrons from the nuclei in the presence of the electromagnetic field^[1].

Mie applied Maxwell's equation with appropriate boundary conditions for an electromagnetic wave interacting with small spheres with the assumption that dielectric constant is not size dependent. The exact solution explains the interaction of light with metallic nanoparticles. If nanoparticles are much smaller than the wavelength of the light ($2r \ll \lambda$) only dipole oscillations contribute to the extinction cross section and then, the Mie theory reduces to the following simple relationship:

$$\sigma_{\text{ext}}(\omega) = 9 \frac{\omega}{c} \epsilon_m^{3/2} V \frac{\epsilon_2(\omega)}{[\epsilon_1(\omega) + 2\epsilon_m]^2 + \epsilon_2(\omega)^2} \quad \text{B.1}$$

where V is particle volume, ω is angular frequency of the incident light, c is velocity of light in surrounding medium, ϵ_m and $\epsilon(\omega) = \epsilon_1(\omega) + i2\epsilon_2(\omega)$ are dielectric

functions of the medium and the nanoparticle material respectively. If ε_2 is neglected, at resonance $\varepsilon_1(\omega) = -2\varepsilon_m$. The above expression is commonly used to explain absorption spectra of small metallic nanoparticles ($2 < 2r < 20$ nm). If size of nanoparticle is more; then, the dipolar approximation is no longer valid and plasmon resonance depends on the size of the particles. As the size of the particle increases higher order modes become important and these modes peak at lower energies. Therefore the absorbance peak moves towards the higher wavelengths ^[2].

B.1 References

- [1]. K. L. Kelly, E. Coronado, L. L. Zhao, and G. C. Schatz (2003) The Optical Properties of Metal Nanoparticles: The Influence of Size, Shape, and Dielectric Environment. J. Phys. Chem. B 107: 668-677.
- [2]. S. Link and M. A. El-Sayed (2000) Shape and size dependence of radiative, non-radiative and photothermal properties of gold nanocrystals. Int. Reviews in physical chemistry 19 (3): 409-453.

Appendix C

SEM images of the nanoparticles

Without PVP

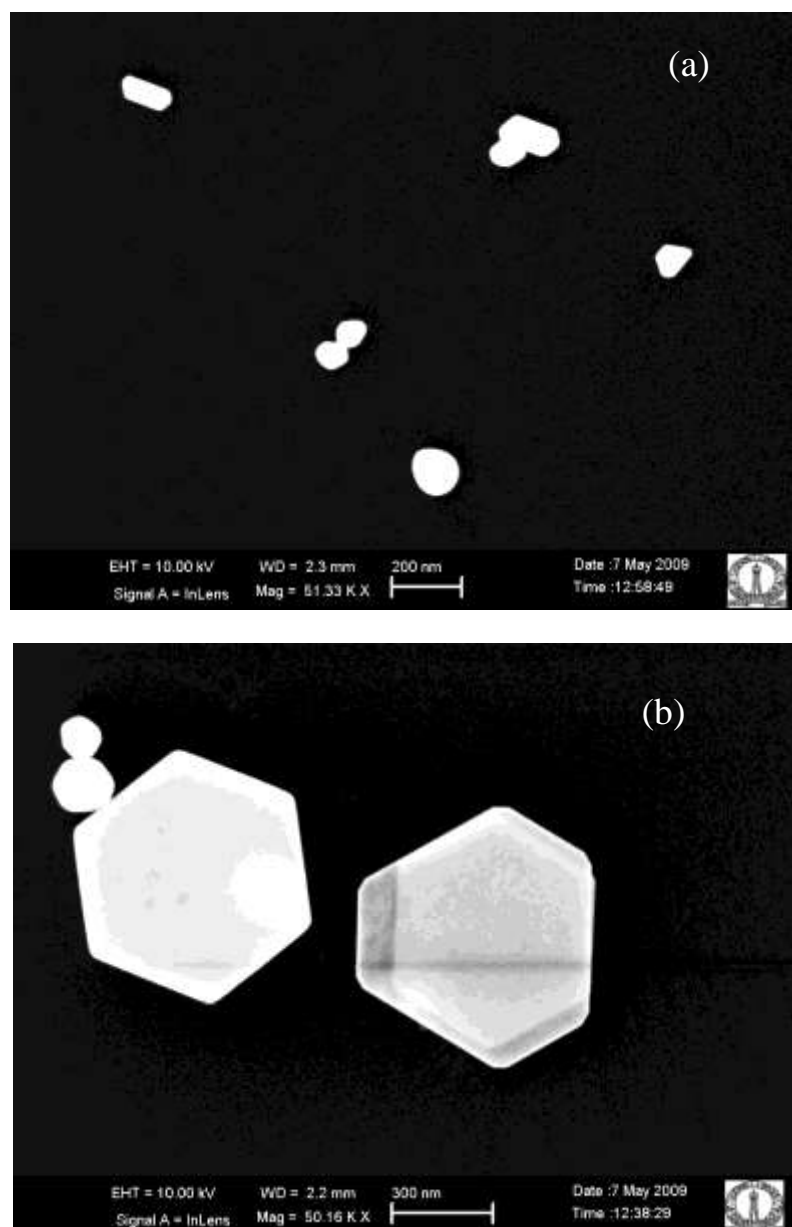


Fig. C.1 SEM images of the gold nanoparticles obtained by citrate method. a). MR 0.6 b). MR 1.5.

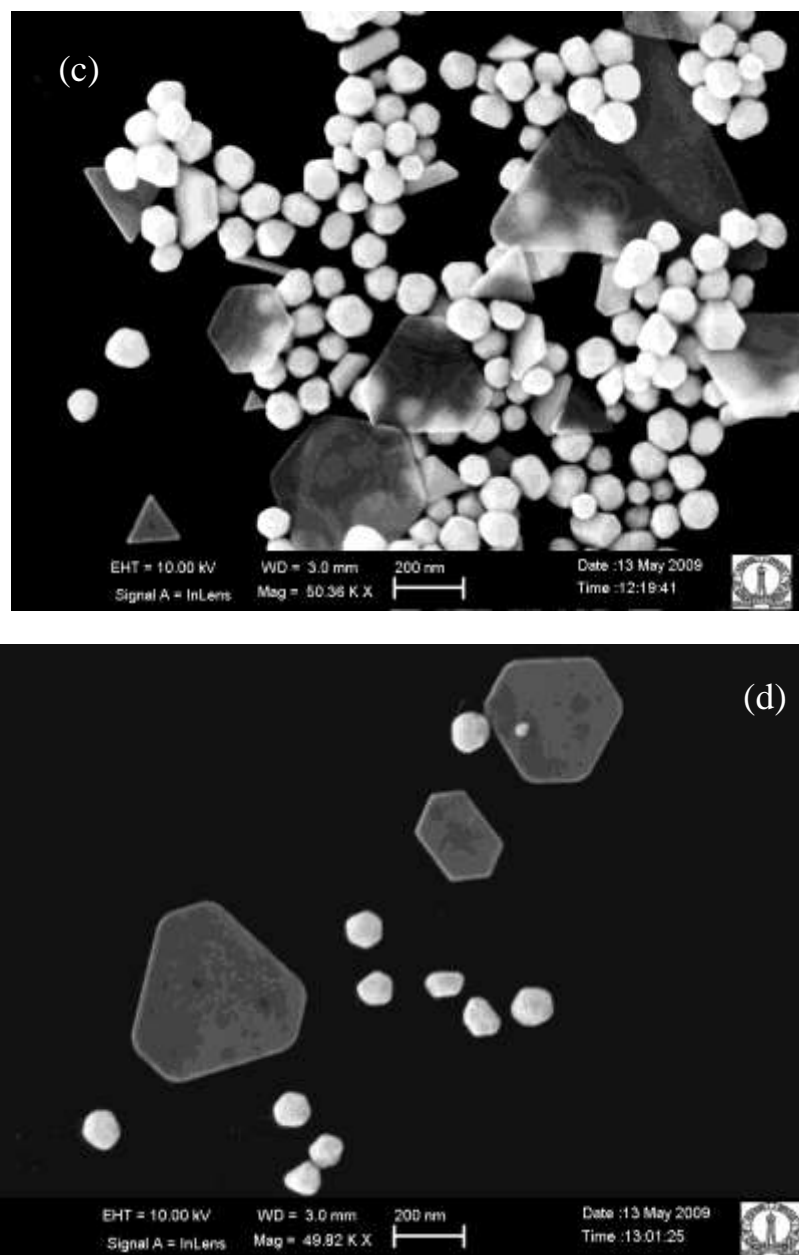


Fig. C.2 SEM images of the gold nanoparticles obtained by citrate method. a). MR 3.5 b). MR 5.2.

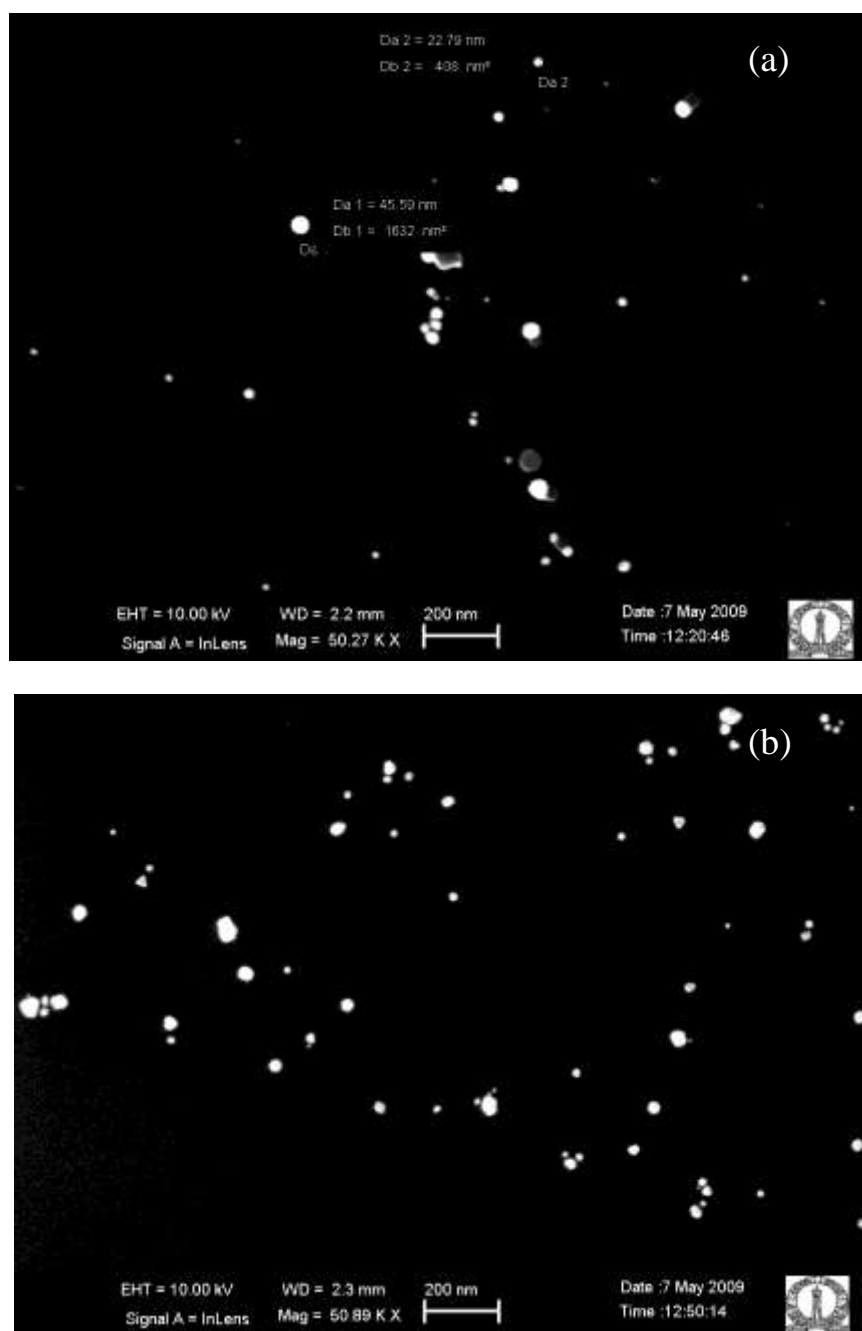
With PVP

Fig. C.3 SEM images of the gold nanoparticles obtained by citrate method. a). MR 0.6 b). MR 1.5.

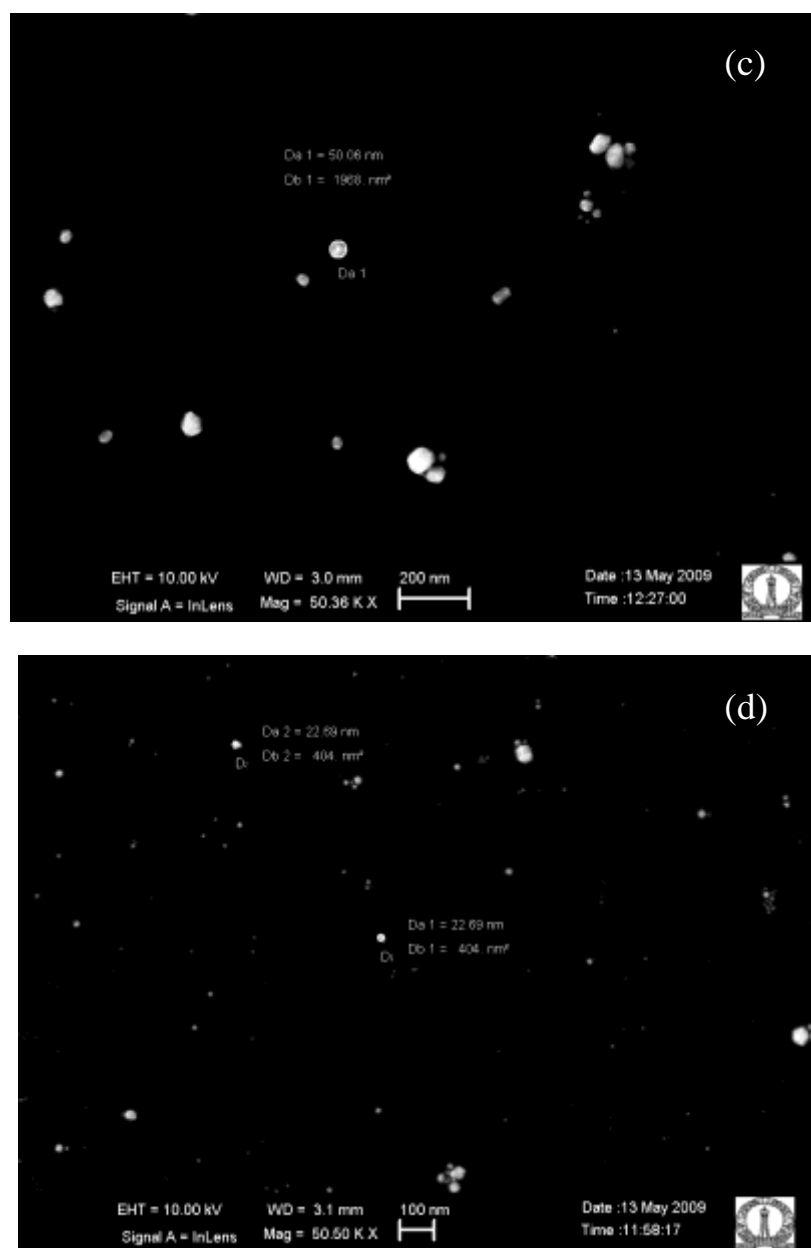


Fig. C.4 SEM images of the gold nanoparticles obtained by citrate method. a). MR 3.5 b). MR 5.2.

Appendix D

Optimization of the model parameters

Best model parameters values were obtained by fitting model predictions to experimental data using Berkeley Madonna software.

D.1 Parameters by fitting predictions at multiple concentrations

Model predictions were tried to fit evolution curve and number density for all concentrations other than 0.065 mM concentration of HAuCl_4 . Until and unless mention orders of the reaction with respect to tannic acid and chloroauric acid taken in model are 1 and 1.5 respectively. During fitting for all concentrations including 0.065 mM concentration floating point error problem faced. The final curve fits and corresponding parameter values are shown in figure C.1 and table C.1 respectively. Model is predicting experimental observations very well at final time, but, at initial time it is over predicting. The reason may be the following. The absolute value of absorbance at lower times is very low compared to the absorbance at final time. Due to this fact, even though the model is over predicting at lower time, the sum of the squares of deviation is less.

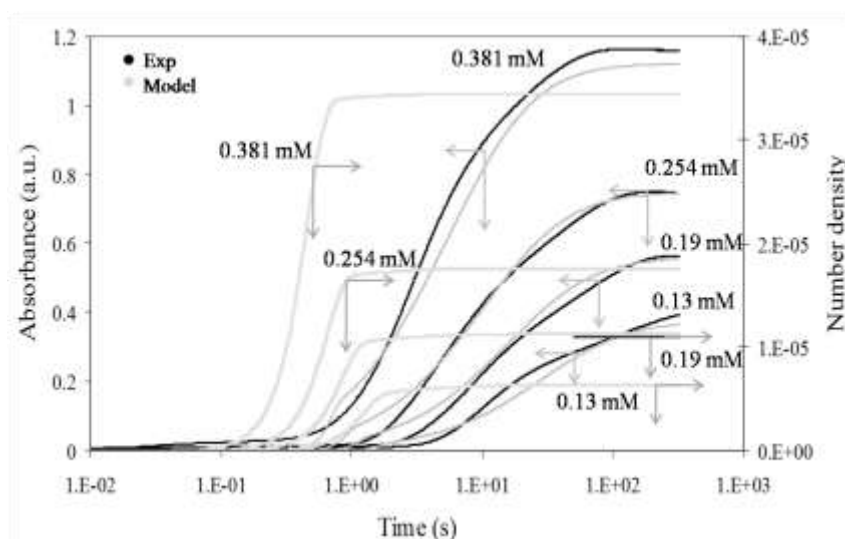


Fig. D.1 Final curve fits for various concentrations other than 0.025 mM concentration at optimized parameters

Parameter	Value	Units
k_r	0.122	$(\text{mol/m}^3)^{-1.5} \text{s}^{-1}$
k_g	1.6	$\text{mol/m}^2 \text{s}$
k_d	0.002	mol/m^3
k_n	4.35	s^{-1}
k_l	2	m/s

Table D.1 Optimized parameter values for the case of multiple curve fitting

D.2 Parameters by fitting normalised absorbance data at multiple concentrations

To get model parameters which follow experimental data at short times also normalised absorbance evolution curves at various concentrations were tried to fit. The final curve fits and corresponding parameter values are given in figure C.2 and table C.2. These parameters are almost same as those parameters for the case of fitting without normalization and predicting experimental data also same way.

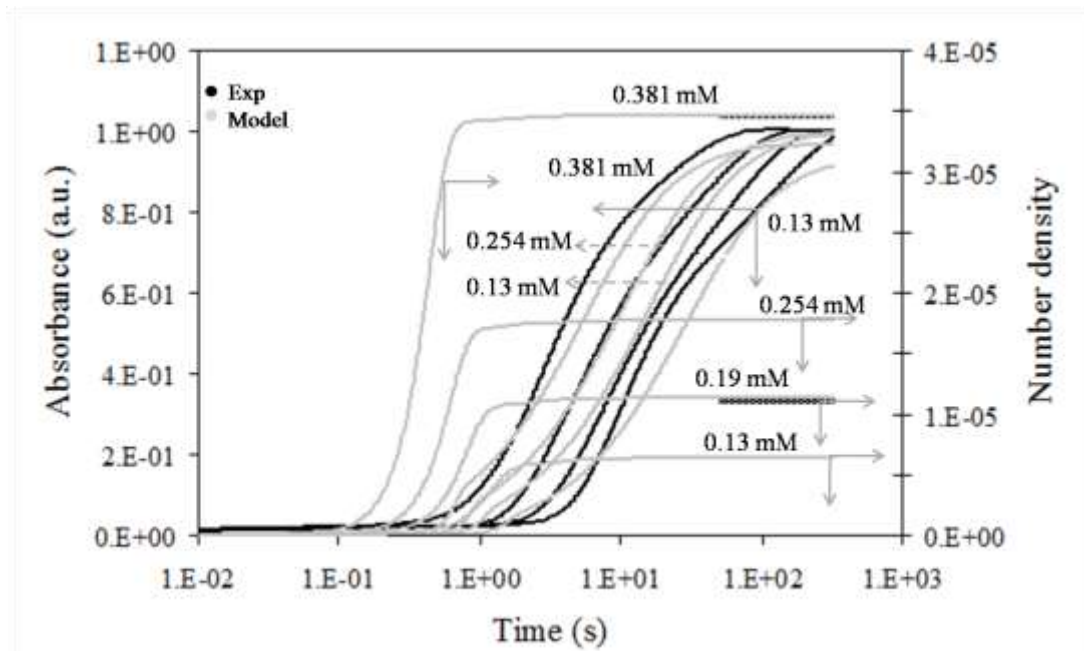


Fig. D.2 Final curve fits for fitting normalised absorbance evolution curves at various concentrations other than 0.025 mM concentration at optimized parameters.

Parameter	Value	Units
k_r	0.122	$(\text{mol/m}^3)^{-1.5} \text{s}^{-1}$
k_g	1.6	$\text{mol/m}^2 \text{s}$
k_d	0.002	mol/m^3
k_n	4.9	s^{-1}
k_l	2	m/s

Table D.2 Optimized parameter values for the case of fitting normalised absorption evolution curves at various concentrations other than 0.065 mM concentration.

D.3 Parameters by fitting predictions at one concentration

Best parameter values were obtained by fitting model predictions at 0.254 mM concentration to the experimental data. The final curve fit and corresponding parameter values are shown in figure C.3 and table C.3 respectively. The same parameters were used to get predictions at other concentrations. With these parameters, at short times model is under predicting experimental data for higher concentration. To get parameters which predicts at short times also, inverse of absorbance evolution data was tried to fit. But, floating point error problem faced during fitting. The experimental data up to 0.3 s seems to be too noisy, so, model prediction was fitted starting from 0.3 s to the final time. Parameters obtained by this way are same as those parameters obtained by fitting from start of the evolution data. To follow evolution curve at short times for higher concentration, nucleation rate constant should be increased to around 5 s^{-1} from 0.36 s^{-1} .

Parameter	Value	Units
k_r	0.105	$(\text{mol/m}^3)^{-1.5} \text{s}^{-1}$
k_g	2.7×10^{-4}	$\text{mol/m}^2 \text{s}$
k_d	0.024	mol/m^3
k_n	0.36	s^{-1}
k_l	2	m/s

Table D.3 Optimized parameter values obtained by fitting model predictions and experimental data for the case of 0.254 mM HAuCl₄ concentration.

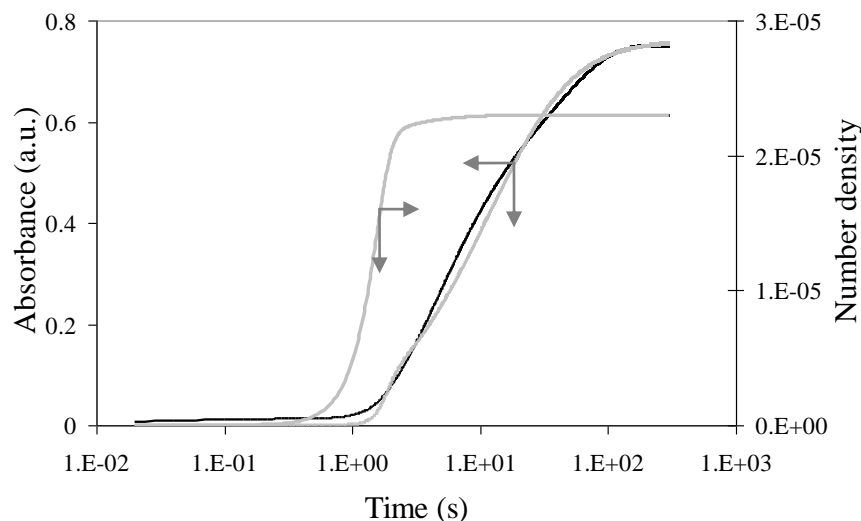


Fig. D.3 Final curve fit obtained by fitting model predictions and experimental data for the case of 0.254 mM HAuCl_4 concentration.

We expected that the parameters which obtained by fitting model predictions of 0.381 mM concentration to the experimental data can predict experimental data at other concentrations well. Parameter values were obtained by fitting model predictions to evolution curve for 0.381 mM concentration. The final curve fit and corresponding parameter values are shown in figure C.4 and table C.4. But, these parameters were over predicting absorption evolution curves for lower concentrations. To predict properly at lower concentrations with these parameters, nucleation rate constant (k_n) should be decreased. So, to predict at all concentration range of interest with order of reactions with respect to tannic acid and chloroauric acid at 1 and 1.5 respectively, optimum k_n should be selected.

Parameter	Value	Units
k_r	0.141	$(\text{mol}/\text{m}^3)^{-1.5} \text{s}^{-1}$
k_g	0.00114	$\text{mol}/\text{m}^2 \text{s}$
k_d	0.019	mol/m^3
k_n	13.8	s^{-1}
k_l	2	m/s

Table D.4 Optimized parameter values obtained by fitting model predictions and experimental data for the case of 0.381 mM HAuCl_4 concentration.

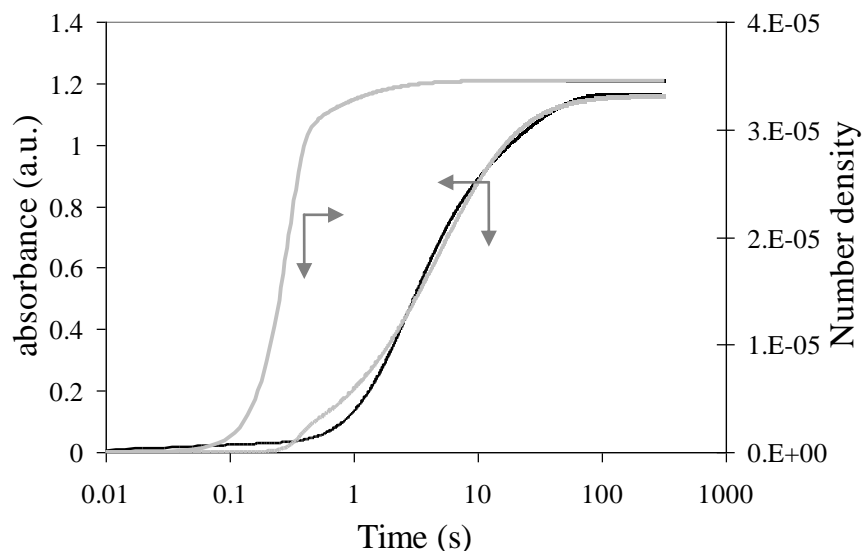


Fig. D.4 Final curve fit obtained by fitting model predictions and experimental data for the case of 0.381 mM HAuCl_4 concentration.

An attempt was made to check the ability of parameters which are obtained by changing order of the reaction to 2 with respect to HAuCl_4 and keeping the same with respect to tannic acid to predict experimental observations at all concentrations. Best parameter values were obtained by fitting model predictions to experimental data for 0.254 mM concentration. The final fit and corresponding parameters are shown in figure C.5 and table C.5. With these parameters model is over predicting experimental observations at short times.

Parameter	Value	Units
k_r	0.34	$(\text{mol}/\text{m}^3)^{-1.5} \text{s}^{-1}$
k_g	9.63	$\text{mol}/\text{m}^2 \text{s}$
k_d	0.015	mol/m^3
k_n	14.9	s^{-1}
k_l	2	m/s

Table D.5 Optimized parameter values obtained by fitting model predictions and experimental data for the case of 0.254 mM HAuCl_4 concentration.

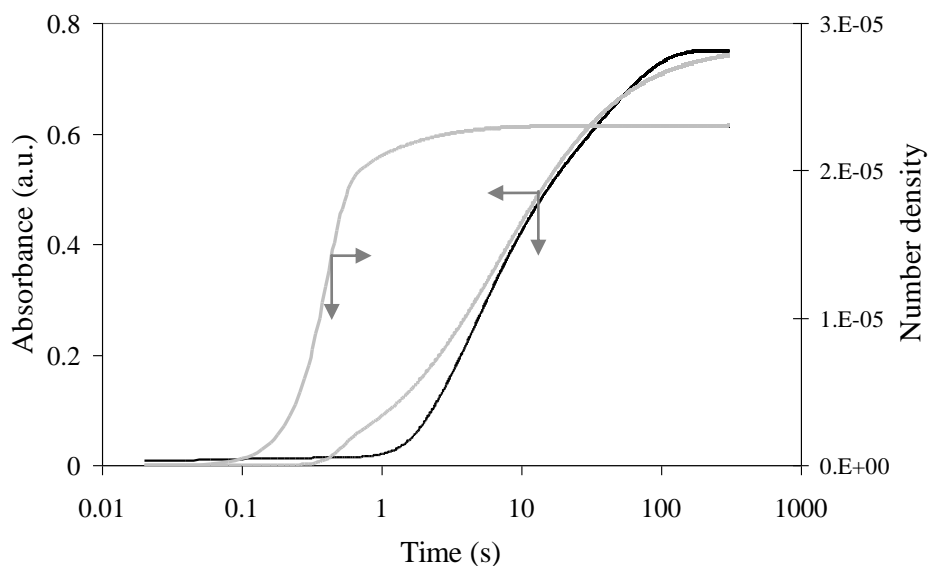


Fig. D.5 Final curve fit obtained by fitting model predictions and experimental data for the case of 0.254 mM HAuCl_4 concentration.

The nucleation rate constant (k_n) was fixed and other parameters were obtained by fitting model predictions to experimental data for 0.254 mM concentration. The final fit and corresponding parameter values are shown in figure C.6 and table C.6. These parameters were predicting experimental observations at other concentrations also well.

Parameter	Value	Units
k_r	0.101	$(\text{mol}/\text{m}^3)^{-1.5} \text{s}^{-1}$
k_g	4.0×10^{-4}	$\text{mol}/\text{m}^2 \text{s}$
k_d	0.009	mol/m^3
k_n	5	s^{-1}
k_l	2	m/s

Table D.6 Optimized parameter values obtained by fitting model predictions and experimental data for the case of 0.254 mM HAuCl_4 concentration.

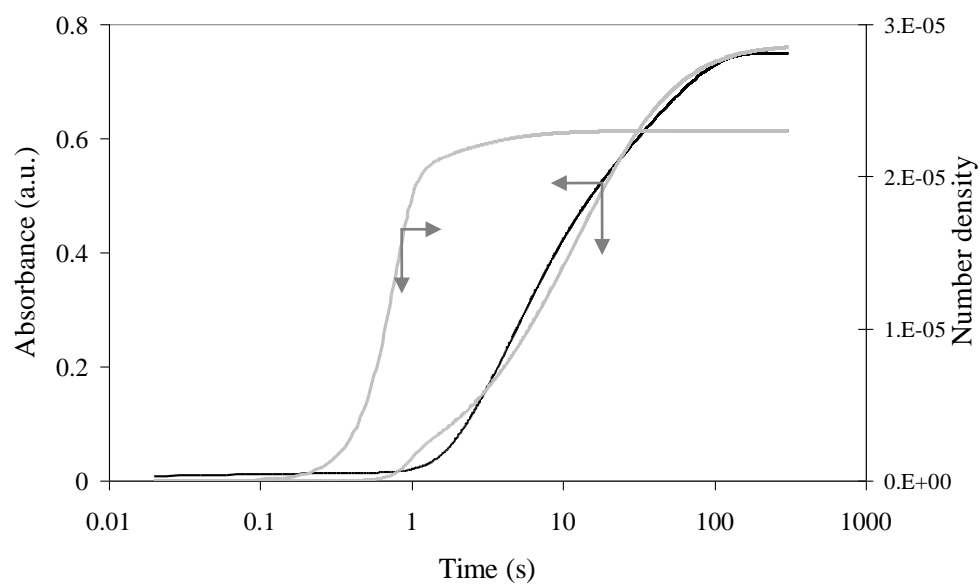


Fig. D.6 Final curve fit obtained by fitting model predictions and experimental data for the case of 0.254 mM HAuCl_4 concentration.

Appendix E

SFM Coupled with Diode Array Spectrophotometer Operation Manual

E.1 Procedure during start up

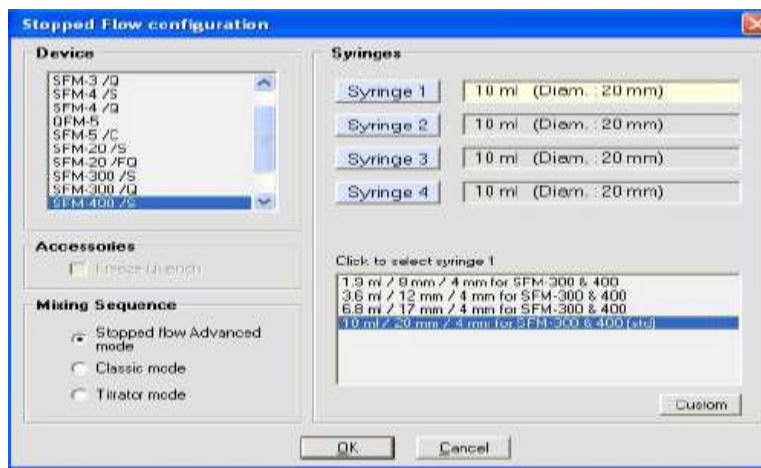
1. Switch on MPS and PC.
2. Start the software by clicking the Biokine icon on the desktop. The following main window will open.



3. From tool bar click on “Install → Device installation”. The following sub window will open.




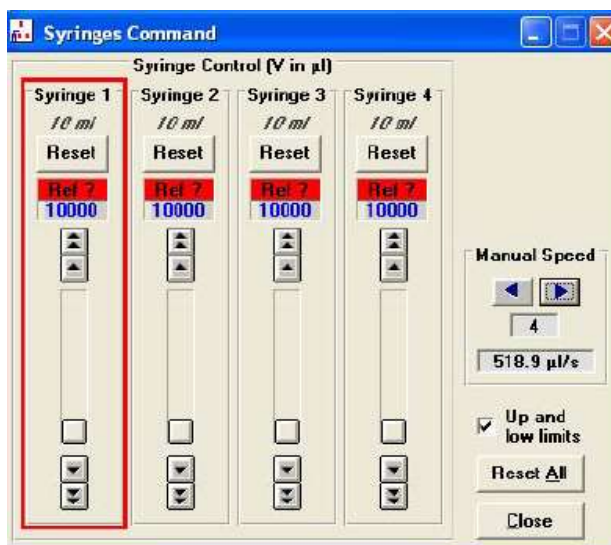
4. Select TIDAS diode array, Use stopped flow and Serial port COM 1. Then, click on “OK”.
5. Again from tool bar click on “Install→ Stopped flow configuration”. The following sub window will open.



6. Select “SFM-400/S”, “Stopped flow advanced mode”, and “10 mm/ 20 mm/ 4mm for -300&400(std) for all syringes. Then, click on “OK”

E.2 Controlling and initializing syringes

1. Click on “” button in the stopped flow status area. The following sub window will open.



2. Bring all syringes to up position using the “up” button on MPS unit.
3. Click on “reset all”→ all syringes are reset.
4. Adjust manual speed to 4 ml/s (advised for 10 ml syringes in manual).

5. Attach a syringe (disposable plastic syringes may be used) containing sample or buffer to a syringe reservoir port on top of the SFM.
6. Set the syringe valve handle to **(R)** and fill the syringes manually, while exerting a slight pressure on the reservoir syringe.
7. Eliminate any bubbles in the SFM syringe by driving the SFM syringe up and down several times while it is connected to the reservoir syringe.
8. Turn the syringe valve handle to **(C)**.
9. Empty one or two elementary movements of the syringe, till you observe liquid flowing out. (to definitively eliminate any bubbles remaining in SFM and cuvette).
10. Repeat the above process for the other syringes.
11. It is recommended that the syringes be filled in reverse numerical order to best remove bubbles from the SFM and cuvette.

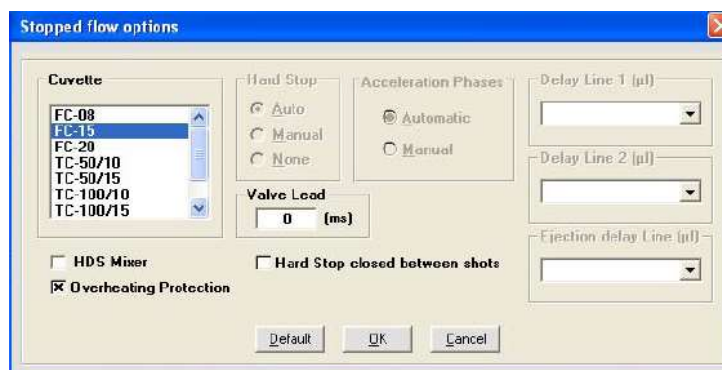
E.3 Stopped flow sequence/ mixing sequence

1. Click on “Mixing sequence” button in the stopped flow status area. The following window will appear.

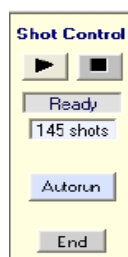
Mixing ratio		Volume		Total flow rate	
S1	2	Total volume / shot	252 µL	S1	101 µL 2.40 mL/s
S2	2			S2	101 µL 2.40 mL/s
S3	0			S3	0 µL 0 mL/s
S4	1			S4	50 µL 1.20 mL/s
				Total flow rate: 6.00 mL/s	

Configuration			
	Content of syringes	Initial concentration	Final concentration
Syringe 1	10 ml		
Syringe 2	10 ml		
Syringe 3	10 ml		
Syringe 4	10 ml		

2. First operation should be to check the configuration of the stopped flow; it is made by clicking on the **SFM Options** button. The following window will appear.

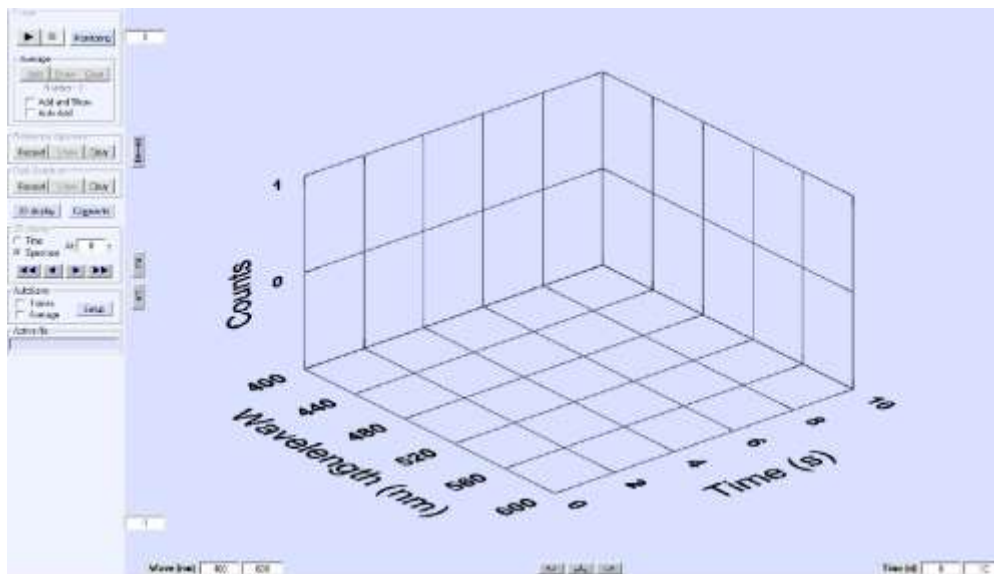


3. Select the cuvette and mixer according to the cuvette and mixer installed in the SFM (don't check HDS mixer), valve lead=0. Then, click on "OK".
4. Set mixing ratio according to concentration required.
5. Adjust the total volume by up or down arrows. The volume from each syringe is automatically calculated. Adjust according to color codes.
6. Total flow rate must be selected using 'up' and 'down' arrows. Once the total flow rate selected the flow rate for each syringe is automatically calculated. Adjust according to color codes.
7. In start of data acquisition click on "At stop".
8. Enter syringe contents and concentrations. The final concentrations are automatically calculated.
9. Click on "Ready"
10. In stopped flow menu bar, the following shot control window will appear (number of possible shots is visible there).



E.4 Operation procedure for diode array spectrophotometer

1. Click on "Device → Diode array spectrophotometer". The following sub window will open.



- Click on Acquisition set up. The following sub window will open.

Diode Array Setup

Scan parameters:

Scan Mode: Absorbance ☒ Trigger

Wavelength from: 255.06 to 728.37 nm [186.5769 - 728.3778 nm]

Integration time: 2 ms [0.8 - 32 ms]

Shutter Mode: Open for scan

Time base:

☐ 1 ☐ 2 ☒ 3 Delay between measurements: 1.0 s (single baseline only)

Number of measurement	Averages / Measurement	Measurement time (ms)	Start (ms)	Stop (ms)
3500	100	200	0	720000
0	0	0	720000	720000
0	0	0	720000	720000

Total measurement time : 12 min 0 s

OK Cancel

- Select scan mode, wavelength range, integration time, shutter mode (If you are controlling light source shutter, Diode array shutter mode should be open for scan; otherwise any shutter mode can work) and number of time base and their parameters. Mark trigger. Click on “OK”.
- Perform dark current measurement by closing the light source shutter and

-Dark Spectrum-

Record Show Clear

click on the record from . The dark current measurement will be displayed on the screen.

5. Inject solvent into the cuvette. Perform reference spectrum by opening the



- light source shutter and click on record from . The lamp spectrum will be displayed on the screen. (Dark spectrum and reference spectrum can be taken only in 2D display mode).
6. Click on auto run from stopped flow menu bar. Send enough shots to make sure that all flow lines are filled with reagents. Then, click on end in auto run window.
 7. Click on the start button of the scope (the message waiting for trigger is displayed in red).
 8. Click on the start button of the shot control window to send a shot. Then, measurement in progress will be displayed on the screen. After measurement results will display on the screen.
 9. To save data click on file from tool bar, select save as and choose drive to save your data at appropriate place.